N70-28090
CR-109888

NATIONAL AERONAUTICS AND SPACE ADMINISTRATION

AN ANALYSIS OF METHODS FOR CALIBRATING THE 13.3 GHz SCATTEROMETER

CRES Technical Report 177-1
December 1969
The Center for Research
University of Kansas

Supported by NASA Manned Spacecraft
Center Contract NAS9-10261

MANNED SPACECRAFT CENTER
HOUSTON, TEXAS

CRES CENTER FOR RESEARCH, INC. · ENGINEERING SCIENCE DIVISION
THE UNIVERSITY OF KANSAS · LAWRENCE, KANSAS · 66044

AN ANALYSIS OF METHODS FOR CALIBRATING THE 13.3 GHz SCATTEROMETER

CRES Technical Report 177-1

G. A. Bradley

The Center for Research
University of Kansas

December 1969

Supported by NASA Contract No. NAS 9-10261

TABLE OF CONTENTS

AN ANALYSIS OF METHODS OF CALIBRATING THE 13.3 GHz SCATTEROMETER

by

G. A. Bradley
The Center for Research
University of Kansas

ABSTRACT

An analysis is presented of dynamic calibration methods that can be used in the 13.3 GHz scatterometer. Four candidate methods are considered with conclusions presented regarding the effectiveness of each method. A mathematical model is derived for each design with the signal frequency spectrum computed at critical points in the receiver. It is shown that the present method of calibration is unacceptable because the calibration signal amplitude is subject to variation. The error in scattering coefficient is shown to be especially sensitive to the bias point and linearity of the ferrite modulator. It is recommended that an injection system be incorporated in the 13.3 GHz scatterometer which uses a square-wave calibration signal. The analysis shows that this method will calibrate the scatterometer to the required accuracy with no error induced in the data record by the calibration system.

Introduction

The 13.3 GHz scatterometer is currently being used in the Earth Resources Aircraft Program to measure and catalog the radar scattering coefficient for various types of terrain. These data will be used as a reference for interpreting future remote radar measurements of the earth; it is therefore essential that the data measured in the present program be calibrated to a known accuracy. This report discusses the calibration requirements of the 13.3 GHz scatterometer and offers detailed mathematical analyses of four candidate methods for calibrating the system.

The radar range equation will be used as a basis for understanding the scatterometer measurement as well as investigating the requirement for calibrating the instrument. The power appearing at the input terminals of the scatterometer receiver is given by the following expression:

$$P_r = K \frac{P_t}{R^4} \sigma \tag{1}$$

where: K = lumped scatterometer system constants

P_t = transmitter output power, in watts

R = radar range, in meters

σ = radar reflection coefficient, in meter^2

The scatterometer system is designed to measure the radar reflection coefficient normalized to the area over which the return power is sampled. Thus, we define

$$\sigma^\circ = \frac{\sigma}{A} \tag{2}$$

where: A = surface area, in meter^2

Suppose now that we wish to calculate the amplitude of the receive power at the output of the scatterometer receiver. If the receiver has a total gain G which includes the amplification or attenuation of each part of the receiver chain, the output of the scatterometer receiver P_r' becomes

$$P_r' = K' \frac{P_t G}{R^4} \sigma^o$$

where: $K' = KA$

The measured scattering coefficient σ^o then becomes

$$\sigma^o = \frac{P_r' R^4}{K' P_t G} \tag{3}$$

To achieve an accurate measurement of the scatterometer coefficient, it is obvious from equation (3) that each term of the expression must be known within the accuracy requirement of σ^o. P_r' is the recorded value of the receiver output power and the accuracy of this term is determined by the known recorder accuracy, integration time, and signal-to-noise ratio. The accuracy of the range term is determined by the accuracy of the aircraft altimeter and knowledge of the position over non-level terrain. The accuracy of the lumped constant K' is known to within the accuracy of the measurement of the various system constants comprising this term. The remaining two terms, P_t, the transmitter output power, and G, the net receiver gain are the variables in the scatterometer which must be monitored by the calibration system. For example, suppose the receiver output signal P_r' suddenly increases. If P_t and G are not monitored and are considered constants, the only conclusion that can be made is an increase in the scattering coefficient σ^o. However, since P_t and

G are variables, a variation in either parameter or in both parameters could account for the increase in P_r'. Therefore, it is necessary to monitor these variables and make appropriate adjustments in the parameters of equation (3) in order to obtain an accurate measurement value for the scatterometer coefficient $\sigma°$.

All techniques for calibrating the scatterometer considered in this paper continuously inject a signal proportional to the transmitter output power into the input in the receiver. The signal is recorded on the data tape recorder together with measured data. Any variation of the calibration signal amplitude must be independent of calibration system variables and must indicate variations in the product P_tG of equation (3).

This report presents an analysis of four designs that can be used in the 13.3 GHz scatterometer. The first design is that used in the present system and it is shown in the analysis that the calibration method has basic limitations in providing the required accuracy for the scatterometer measurement. The second design is similar in concept to the present design with the exception that a semiconductor device (PIN diode) is used in place of the ferrite modulator to inject the calibration signal into the receiver. This design has some advantage over the present configuration but still has basic limitations in providing the required measurement accuracy. In the third and fourth designs we propose to change the present microwave configuration such that a transmitter-calibrated signal is coupled into the receiver without affecting the return data signal. The third design uses a sinusoidal signal to produce the calibration signal. The fourth design uses a square wave signal to produce the calibration signal. It is shown in the analysis that the fourth design can provide the required calibration accuracy at the same time that the fundamental accuracy of the measured data is improved by reducing errors due to variations in the phase of the received signal.

The results of the analyses lead to the conclusion that the 13.3 GHz dual-polarized scatterometer should be modified to use the fourth design to assure a high accuracy of the measured data. Further, the enclosed analysis of the present calibration method offers evidence that all past data measured with the present configuration was subject to error in the calibration signal and hence in the absolute level of the scatterometer coefficient data. Because this error is variable, the measured data bias level is also variable. In the case of sea-state data, the homogeneous nature of the scattering surface permits the slope of the scatterometer coefficient data as a function of the incidence angle to be used if the absolute level of the coefficient is ignored. This can only be considered a temporary method of utilizing past sea-state scatterometry data.

It must be strongly emphasized in this introductory material that there is a direct relationship between scatterometer data quality, represented by the accuracy of the recorded measurement, and the method of calibration used in the system. Because of the experimental nature of the scatterometer program, it is imperative that only data of high accuracy be used to evaluate the relationship between radar scattering response and the nature of the measured terrain. It is for this reason that the present scatterometer configuration must be modified to include a calibration network which will assure this accuracy and will, at the same time, be independent of environmental and operational conditions.

Analysis

The operation of four calibration systems suitable for use in the 13.3 GHz scatterometer is analyzed in this paper. The analysis includes the calculation of signal levels and frequency spectral characteristics at key points in the receiver chain for each candidate design. The complete mathematical analyses are presented in Appendices I and II with major results quoted in this section together with a discussion of the techniques and the operational requirements for precise calibration of the scatterometer.

Appendix I considers the present configuration which uses a ferrite modulator in the rf received signal path to insert the calibration signal into the receiver. The material presented in this appendix is also applicable to the second calibration design which replaces the ferrite modulator with a PIN diode modulator. This change does not affect the signal levels nor the spectral behavior of the receiver since the technique is similar to the present technique. The modulator component stability and reliability together with data phase shift characteristics are the only factors to be considered in comparing the two designs.

Appendix II proposes a modification to the 13.3 GHz scatterometer calibration system in which a calibrated sample of the transmit signal is injected directly into the receiver input terminals. The material presented in this appendix considers the use of two different shapes for the calibration control waveform: a sine wave (Design III) and a square wave (Design IV).

Appendix III presents an introduction to the use of PIN diode devices as microwave modulators.

Appendix IV presents an analysis of absorption devices used as modulators in the four calibration system designs. Note I in this appendix considers the modulator bias requirement in relation to the 'gain' transfer characteristic with the error in calibration signal amplitude calculated as a function of the bias level. Finally, Note II of the appendix considers the error in the calibration signal when a non-ideal square wave is used in the signal injection system.

Design 1 - Present system: ferrite modulator

Consider first the calibration system presently in use in the 13.3 GHz scatterometer. Figure 1 shows a block diagram of the system. A brief explanation of the operation of the system is necessary in order to understand the operation of the calibration technique. The 13.3 GHz transmitter continuously emits energy from the transmitter antenna at the same time that attenuated samples of this energy are directed to the receiver for use in the calibration system as well as in the mixer. The receiver operates continuously with the rf received energy passing through a power divider - hybrid arrangement which shifts the phase of one output of the divider by 90° with respect to the second output. The rf phase shift provides a capability for separating positive and negative Doppler frequencies (corresponding to fore and aft data, respectively) after the spectral folding which occurs in the mixer. The receive signal without phase shift is passed through a directional coupler which adds an attenuated (36.5 dB) sample of transmit energy to the data frequency spectrum. Following the coupler, the modified receive signal is amplitude modulated at the calibration signal frequency (usually 10 to 12.5 kHz) by using a ferrite modulator. This ferrite modulator can be considered as a variable attenuator using the properties of the ferrite material to adjust the 'gain' (≤ 1) experienced by the rf energy. The modulated data signal, in parallel with the phase-shifted signal is then mixed down to dc followed by amplification and recording of the information. The essential elements of the scatterometer system that must be considered when analyzing the calibration technique include the directional coupler, the

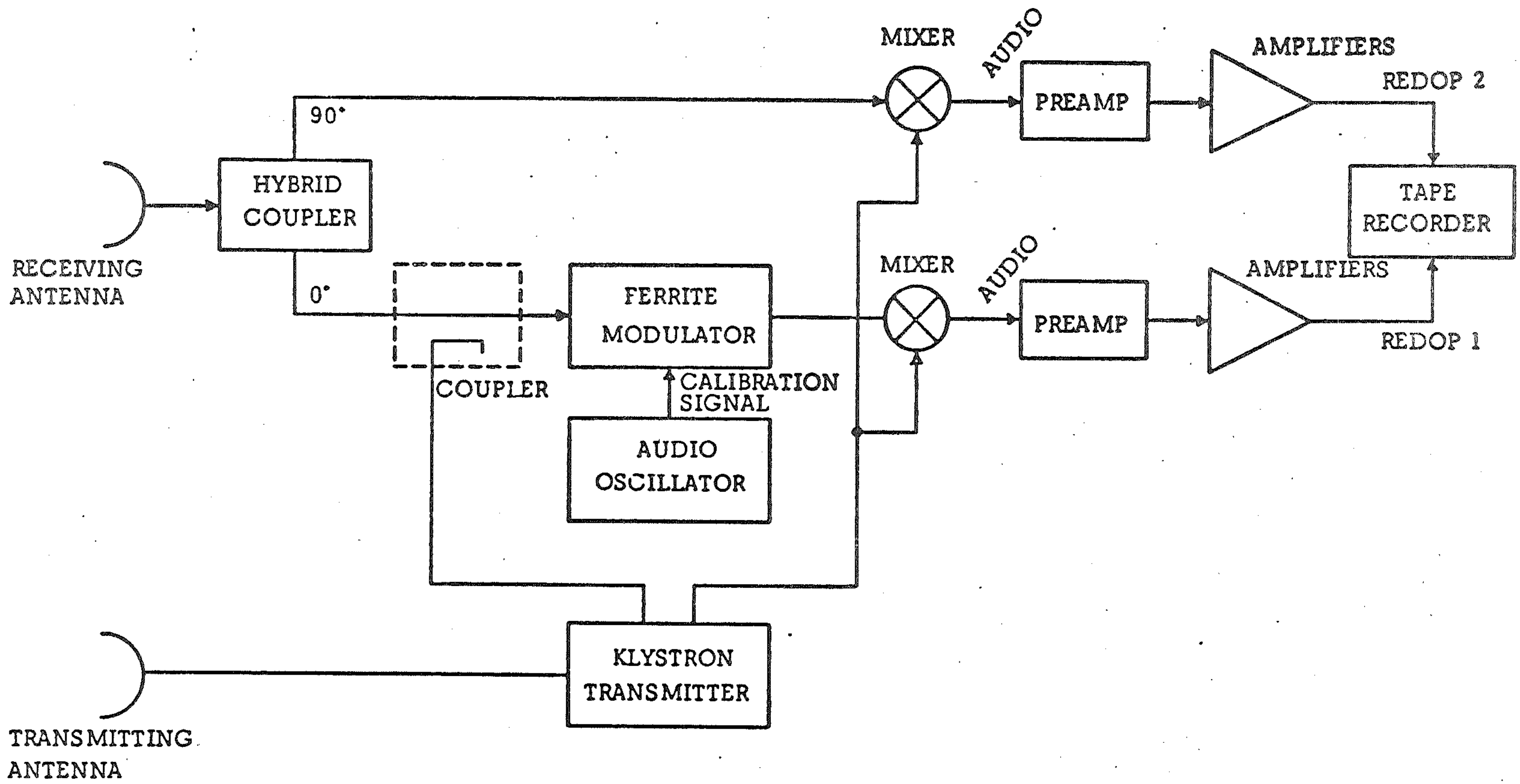

FIGURE 1: 13.3 GHz RADAR SCATTEROMETER BLOCK DIAGRAM

ferrite modulator, the audio oscillator and the mixer.

Figure 2 shows the frequency spectrum of the receiver at (a) the input to the directional coupler, (b) the output of the coupler, (c) the output of the ferrite modulator, and finally at (d) the output of the mixer. The following definitions of the several signals are appropriate to the following analysis.

A_l:	y_l	=	$A_l \cos \omega_o t$	(leakage from transmitter)
A_s:	y_s	=	$A_s \cos (\omega_o + \omega_d)t$	(return Doppler signal)
A_t:	y_t	=	$A_t \cos \omega_o t$	(coupled transmitter sample)
A_c:	y_c	=	$A_c \cos \omega_c t$	(calibration oscillator output)
A_x:	A_x	=	$A_t + A_l$	(total transmitter sample)
α_o:	α_o	=	quiescent 'gain' of the ferrite modulator	
α_m:	α_m	=	transfer 'gain' characteristic of the ferrite modulator	
ω_o:	ω_o	=	frequency of the transmitter, in radians/second	
ω_d:	ω_d	=	Doppler frequency of the return signal, in radians/second	
ω_c:	ω_c	=	frequency of the calibration oscillator, in radians/second	

Figure 2(a) shows the frequency spectrum at the receiver input. The amplitude of the Doppler-shifted return signal spectrum is shown constant for illustrative purposes but, in general, will vary depending on the return from specific incident angles. For our analyses we will consider only one Doppler component at frequency ($\omega_o + \omega_d$) as indicated in the figure. The input spectrum contains, in addition to the signal spectrum, a component at the transmitter frequency due to leakage between the transmit and receive antennas and microwave circuitry. On the figure, this is represented as A_l.

The purpose of the directional coupler is to inject an attenuated sample of the transmitter output into the receive spectrum. The result of this operation is shown in (b) where the coupled signal A_t is added to the leakage signal to

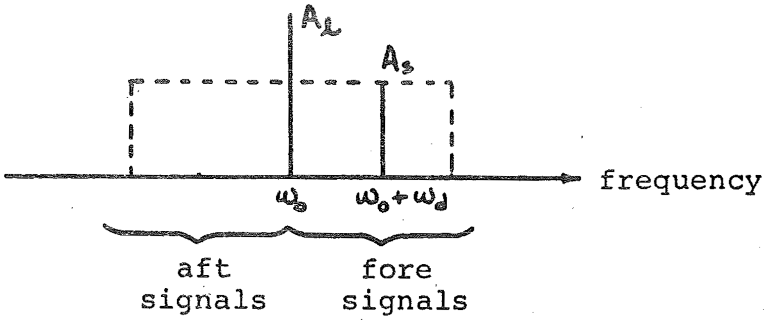

(a) Spectrum at input to the directional coupler.

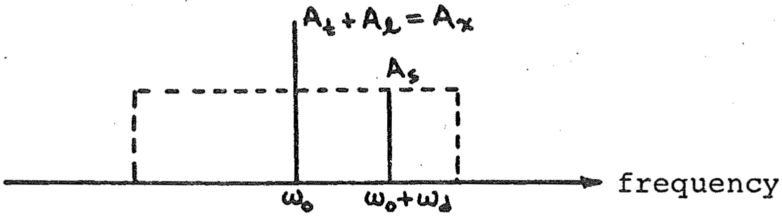

(b) Spectrum at output of the directional coupler.

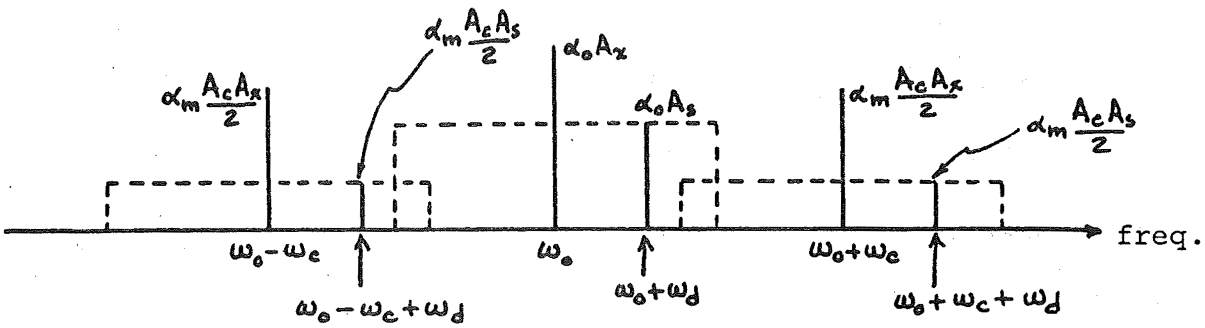

(c) Spectrum at output of the ferrite modulator.

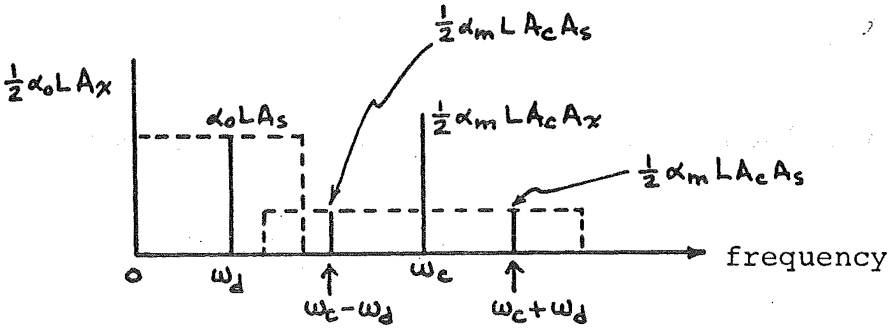

(d) Spectrum at output of mixer.

Figure 2: Frequency spectrum in the present 13.3 GHz scatterometer configuration.

produce a net component A_x at the transmitter frequency ω_o. (This assumes the phase between A_t and A_l is zero with no attenuation of the signal through the directional coupler.)

Figure 2(c) shows the spectrum at the output of the ferrite modulator. In order to understand this rather complex spectrum we will consider the process of variable 'gain' used by the ferrite device to achieve modulation. A detailed analysis of the modulation process, given in Appendix IV, shows that, given a proper bias point α_o and a constant gain slope α_m, then the total gain of the ferrite modulator (see equation N1-4) is that given in the expression below.

$$y''_{rf} = \alpha \left[A_x \cos \omega_o t + A_s \cos (\omega_o + \omega_d) t \right] \tag{4}$$

where: α = total 'gain' of the ferrite modulator

$= \alpha_o - \alpha_m A_c \cos \omega_c t$

The expression in equation (4) can be rewritten as equation (5) below using the appropriate trigonometric relations.

$$\begin{aligned} y''_{rf} = {} & \alpha_o \left[A_x \cos \omega_o t + A_s \cos (\omega_o + \omega_d) t \right] \\ & - \alpha_m \left[\tfrac{1}{2} A_c A_x \cos(\omega_o + \omega_d) t + \tfrac{1}{2} A_c A_x \cos (\omega_o - \omega_c) t \right] \\ & - \alpha_m \left[\tfrac{1}{2} A_c A_s \cos (\omega_o + \omega_c + \omega_d) t + \tfrac{1}{2} A_c A_s \cos (\omega_o - \omega_c + \omega_d) t \right] \end{aligned} \tag{5}$$

The spectrum in Figure 2(c) shows the frequency components of equation (5) with terms appearing at the transmit frequency, the Doppler-shifted signal frequency, the carrier frequency plus-and-minus the calibration oscillator frequency, and signal sidebands of the last term displaced by the Doppler frequency. The appearance of sidebands of the signal around the calibration frequency is disturbing since these terms overlap the signal spectrum. However, an interpretation of this effect will be delayed to the discussion of the audio signal spectrum at the output of the mixer.

Turning now to the output spectrum of the mixer which is the output spectrum of the scatterometer recorded on the data tape recorder, the expression for this signal is given in Appendix I by equation (I-8) and repeated as equation (6) below. It should be pointed out that the terms appearing in the Doppler spectrum of both the signal and the sidebands around ω_c are the sum of fore and aft signals and, for the purpose of this analysis, are assumed equal. In operation, the terms will vary with the expected values indicated in the equation.

$$y_s(t) = \frac{1}{2}\alpha_o L A_x + \alpha_o L A_s \cos\omega_d t - \frac{1}{2}\alpha_m L A_c A_x \cos\omega_c t - \frac{1}{2}\alpha_m L A_c A_s \cos(\omega_c + \omega_d)t - \frac{1}{2}\alpha_m L A_c A_s \cos(\omega_c - \omega_d)t \tag{6}$$

where: L = mixer conversion gain

The first term in equation (6) appears at dc and does not appear at the output of the scatterometer because of the bandpass characteristic of the receiver amplifiers. The second term is the scattering signal information which, when processed, will yield the scattering coefficient data. The third term, and the term of most interest here, is the calibration signal and is used in the data processing operation to indicate variations in the transmitter level and variations in net receiver gain. The fourth and fifth terms are sidebands of the Doppler signal which appear symmetrically about the calibration signal as a result of the modulation performed directly in the signal path.

It is clear from Figure 2(d) that the sideband energy appearing on either side of the calibrate signal must be below the audio noise level N at the output of the mixer in order for the sideband energy not to interfere with the data spectrum. Therefore, if A_x, the total transmitter sample, is much larger than A_s, the Doppler signal, we must adjust the level of A_c such that

$$\frac{1}{2}\alpha_m L A_c A_s < N$$

or

$$A_c < \frac{2N}{\alpha_m L A_s} \tag{7}$$

In practice, the calibrate signal $\frac{1}{2}\alpha_m A_c A_x$ is adjusted by A_c such that the ratio $\frac{\alpha_o A_x}{\frac{1}{2}\alpha_m A_c A_x} = 2\frac{\alpha_o}{\alpha_m}\frac{1}{A_c}$ is 90 dB. Therefore, if the data signal is -60 dBm at zero Doppler frequency, the sideband level around the calibrate signal is -150 dBm which is well below the system noise level of approximately -130 dBm.

If A_c is adjusted according to equation (7), the output spectrum of the scatterometer is that indicated in Figure 3. For the figure, a gain of G is assumed for the receiver stages following the mixer. In addition, the effects of the rolloff function have been ignored since only the lower frequencies in the signal spectrum are affected by this function.

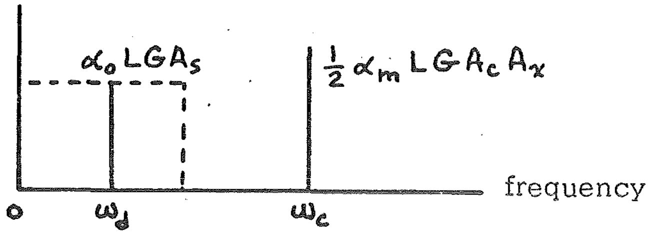

Figure 3: Output spectrum of Redop 1 channel of the 13.3 Ghz scatterometer.

We are now in a position to discuss the calibration method presently used in the scatterometer by reference to Figure 3. The calibration signal $y_c(t)$ is given in equation (8) below.

$$y_c(t) = \frac{1}{2} \alpha_m L G A_c A_x \cos \omega_c t \tag{8}$$

where:

α_m	=	transfer 'gain' of the ferrite modulator
L	=	mixer conversion gain
G	=	gain of the receiver stages following the mixer
A_c	=	peak amplitude of the calibrate signal
A_x	=	total transmitter sample at the output of the directional coupler
	=	$A_t + A_l$
A_t	=	coupled transmitter sample
A_l	=	leakage transmitter signal at receiver input terminals

Equation (8) indicates that the calibration signal recorded on the data tape recorder is indeed a function of the transmitter output level as well as the net receiver gain. However, $y_c(t)$ is also a function of the amplitude of the calibration signal A_c and the slope α_m of the ferrite modulator transfer response. The expression in equation (8) assumes a constant slope α_m where, in fact, α_m is a function of the instantaneous amplitude ($A_c \cos \omega_c t$) of the modulating signal and the bias point α_o. Therefore, any variation in the ferrite modulator operating point and transfer characteristic results in a bias shift of the reduced data.

The transfer 'gain' characteristic of the ferrite modulator is symmetrical about the 'gain' axis (i.e., equal positive and negative modulating fields result in equal transfer 'gains') and, for undistorted operation, the bias point must constrain the modulating operation to one quadrant of the transfer curve. From the detailed analysis of the modulator operation in Appendix IV, it can be concluded that any change in the operating point α_o will cause errors in the calibration signal due to the change in α_m. Further, if operation is forced into the bilateral region of the transfer characteristic, the error increases dramatically because the modulator produces higher harmonic frequency terms with an attendant decrease in the amplitude of the first harmonic at the calibrate frequency. The worst case occurs with the bias α_o at the origin of the modulator transfer curve. Dynamic operation is then symmetric about the origin with only the second harmonic of the calibrate frequency appearing in the output spectrum.

The ferrite modulator, in the present configuration of the 13.3 GHz scatterometer, has no dc bias applied to the modulation signal terminals. This assures a small rf signal insertion loss but requires the modulation function to operate with a bias point determined by the residual magnetism in the ferrite material. As a consequence, any change in residual magnetism due to temperature variations, aircraft vibration, stray magnetic fields or other effects will result in changes in the operating point α_o and the gain slope α_m of the modulator. The result is a change in the calibration signal amplitude with a corresponding change in the scattering coefficient bias level. This unstable situation can explain the σ° bias shift evident on most of the recently measured scatterometry data and should be considered a major limitation in the usefulness of the present 13.3 GHz scatterometer configuration.

In judging the merits of the present calibration method, we must consider the effects of phase shift introduced by the ferrite modulator in one channel of the scatterometer receiver. Again referring to the system block diagram shown in Figure 1, the two receive channels contain identical information with the exception that the Redop 2 channel has a phase shift of 90° with respect to Redop 1. Because the calibration network operates only on the Redop 1 channel, an additional phase difference and attenuation between the two channels results from the ferrite modulator. Therefore, the net phase difference between Redop 1 and Redop 2 is no longer 90° as required for data processing to separate fore and aft data, but is 90° minus the phase shift (assumed positive) introduced by the ferrite modulator. It has been shown[1] that the phase error must be less than 2° in order for the error in calculating σ° to be less than 0.15 dB. Further, since the modulator is sensitive to temperature and vibration changes, it is suspected that phase shift and hence, data processing accuracy, will also be dependent on these environmental fluctuations. The ferrite modulator introduces attenuation in Redop 1 data compared to Redop 2 data. However, this attenuation is compensated for by adjusting the gain of Redop 1 channel such that the two audio output signals are approximately equal. If the output signals do not differ by more than 10%, the data processing program will adjust the amplitude of the two channels to be equal. This assumes a sufficiently high signal-to-noise ratio in both channels with the static ferrite modulator loss included in the calculation for σ°. Table II below lists the requirements for successful use of the present method of calibrating the 13.3 GHz scatterometer.

---

1. Bradley, G. A., "An Analysis of RF Phase Error in the 13.3 GHz Scatterometer," CRES Technical Memorandum No. 118-20, November 1969.

Table II: Requirements for successful calibration of the 13.3 GHz scatterometer using the present method.

Parameter	Requirement
Calibration oscillator signal amplitude: A_c	• $A_c < \frac{2N}{\alpha_m L A_s}$ • amplitude accurately measured • no significant amplitude variations
Ferrite modulator characteristics:	• fixed bias α_o with no variations • α_m accurately measured constant • no variations of phase or attenuation with temperature or vibration
Transmitter leakage: A_ℓ	• accurately measured value • no variations of leakage constant

Design 2 - Present system: PIN diode modulator

The second calibration method substitutes a PIN diode modulator for the ferrite modulator in the present calibration system. The spectral analysis is identical to that for design 1 presented above with the output spectrum as shown in Figure 3 and the calibrate signal given in equation (8). The requirements for successful calibration are the same as listed in Table II. The expected benefit of using a PIN diode modulator compared to the present ferrite modulator is an improvement (i.e., decrease) in the temperature and vibration sensitivity of the device. To accurately determine the advantage of replacing the ferrite modulator with a PIN diode modulator, an extensive environmental testing program will be required for both devices. Because such a testing program has not been performed, no conclusion can be reached as to the advantage of modifying the present configuration to use a PIN diode modulator in place of the ferrite device.

<u>Design 3 - Signal injection: sine wave</u>

The signal injection calibration system modulates a sample of the transmitter signal with a calibration oscillator signal, then simply adds this signal to the incoming rf data signal. The several advantages of this method compared to the present calibration method will be indicated during the course of this analysis.

Figure 4 shows a block diagram of the 13.3 GHz scatterometer system modified to use the signal injection calibration design. This figure should be compared with Figure 1 to understand the differences in the two methods. The injection system removes the modulator from the return rf signal path and instead, adds the calibration signal at rf to the data frequency spectrum. The injected calibration signal is proportional to the transmitter energy since a sample of the transmitter output is used as the carrier in the injection system. The most significant improvement we recognize at this point is the removal of the ferrite device from the signal path. Thus, the dependence of accurate data measurement on modulator phase and amplitude stability is removed. We shall show in the following analysis that another advantage is realized by removing the dependence of the calibrate signal on transmitter leakage.

A complete analysis of the calibration design shown in Figure 4 is presented in Appendix II. Two waveforms for the calibration signal generator are assumed in the analysis. The first waveform is a sine wave with the analysis repeated for a square wave. In this section we shall be concerned with the sine wave output of the calibrate signal generator. It should be mentioned in discussing the block diagram of Figure 4 that the modulator used in the injection system can be either a ferrite modulator or a PIN diode modulator. However, it is expected that increased reliability and independence of environment variations will indicate clear superiority of the PIN diode device in this application.

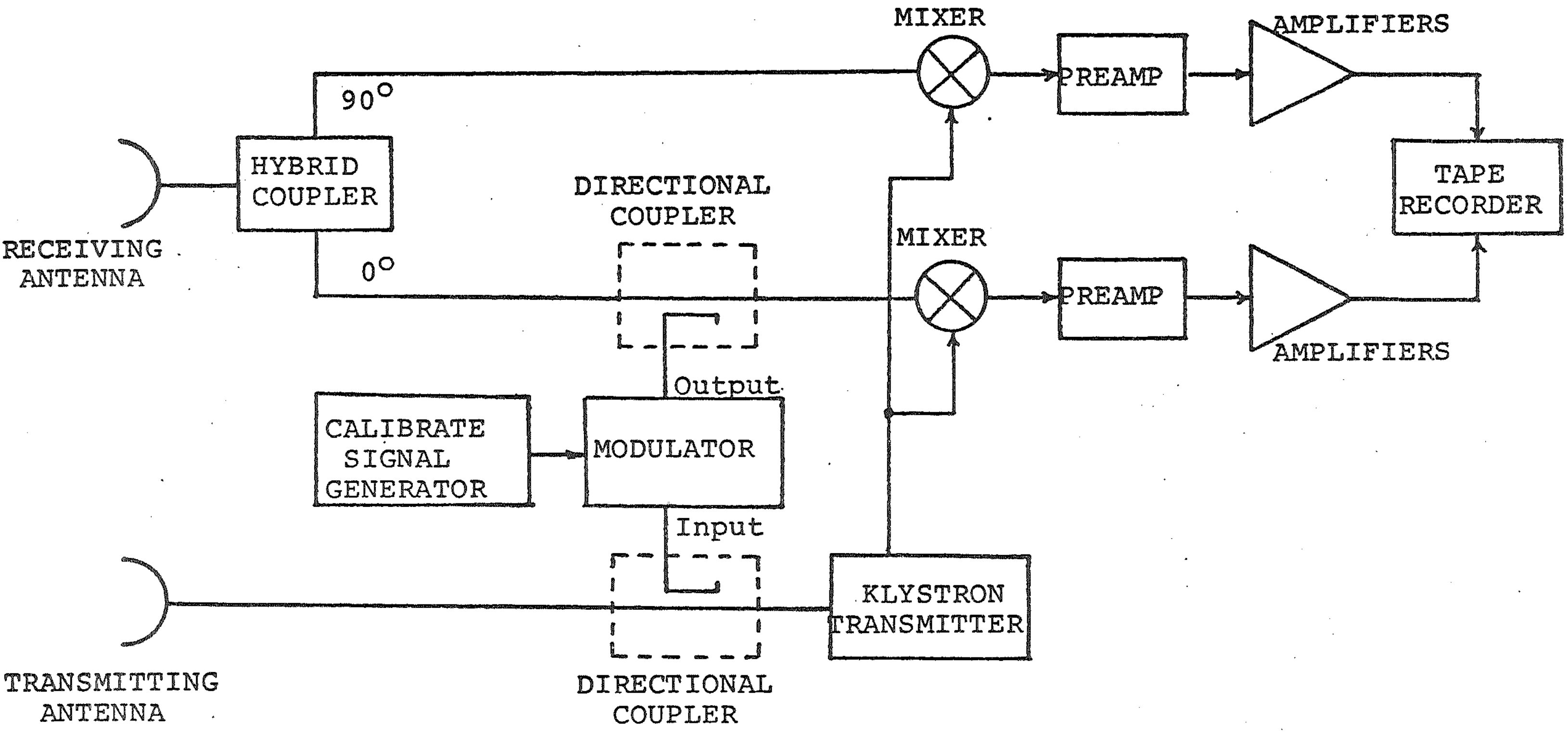

FIGURE 4: 13.3 GHz Scatterometer using calibrate signal injection.

Figure 5 shows the frequency spectrum of the scatterometer system, with sine wave calibration injection, plotted for several key locations in the system. First, consider Figure 5(a) which shows the spectrum at the output of the modulator. The symbols used in the figure are identical to those used in the Design 1 analysis. Figure 5(b) shows the spectrum at the input to the mixer in the receive channel Redop 1. Note that this spectrum is merely the spectrum of the return data signal (containing the Doppler information) modified by the injection of the calibration signal into the spectrum. In the figure, k_2 is the coupling constant of the directional coupler in the receiver line. Figure 5(c) shows the spectrum at the output of the mixer. As before, the fore and aft signals are assumed to be equal with the folded data spectrum appearing as shown in the figure.

Figure 6 below shows the output spectrum of the 13.3 GHz scatterometer using the injection calibration method with sine-wave calibration signal generation. From the figure it is seen that the calibration signal $y_c(t)$ is given by the expression of equation (9) below.

$$y_c(t) = \frac{1}{2} \alpha_m k_2 L G A_c A_t \cos \omega_c t \tag{9}$$

where: k_2 = coupling constant of the directional coupler

remaining terms as defined for equation (8)

Comparing equation (9) with equation (8) shows that the only difference between the two expressions is the additional constant k_2 in equation (9) and the factor A_t instead of A_x. Thus, we can conclude that a slight improvement in the calibrate signal accuracy is obtained by the elimination of the dependency on leakage from the transmitter. However, the scatterometer system data

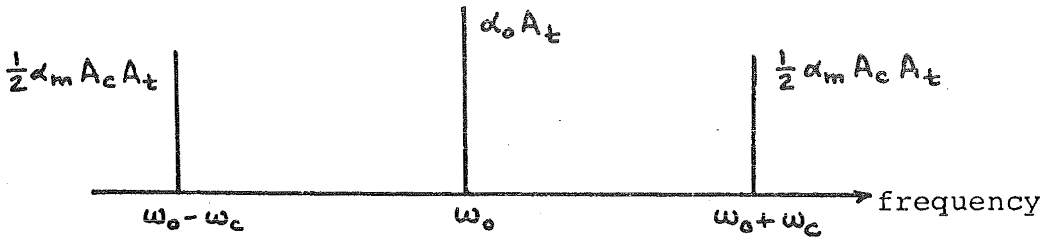

(a) Spectrum at the output of the calibrate signal modulator.

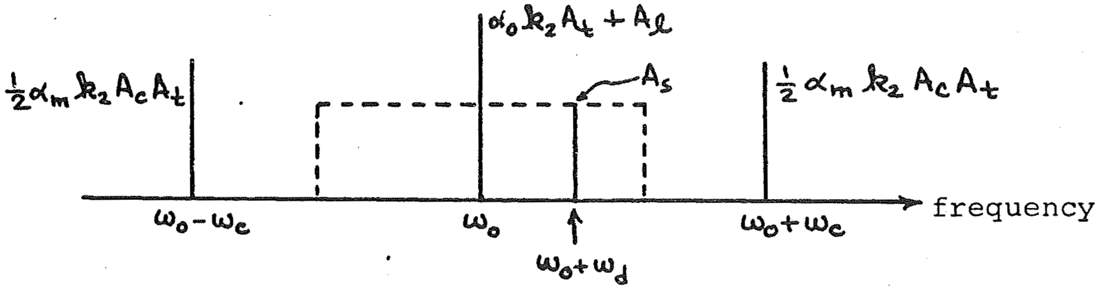

(b) Spectrum at the input to the mixer.

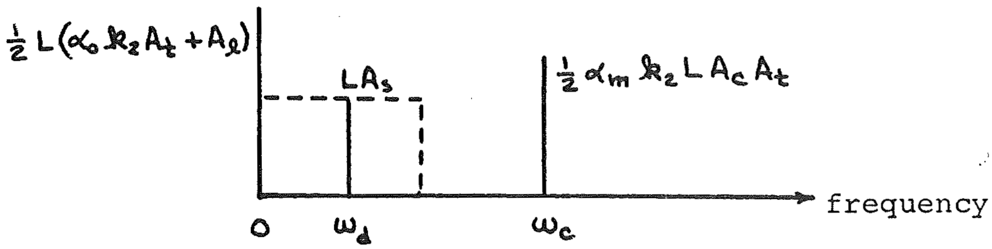

(c) Spectrum at the output of the mixer.

Figure 5: Frequency spectrum in 13.3 GHz scatterometer using signal injection method for calibration. A sine wave is assumed as the calibration signal source.

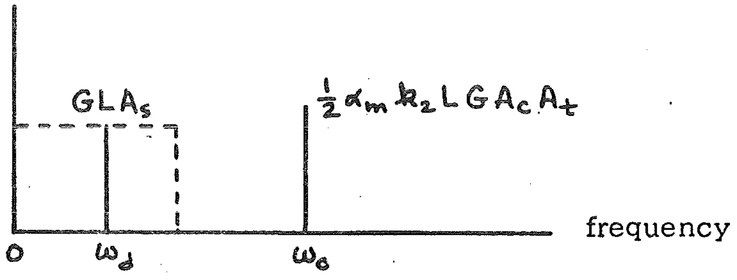

Figure 6: Output spectrum of the 13.3 GHz scatterometer with sine-wave calibration signal injection.

accuracy is improved by removing the modulator from the rf data signal path, thus eliminating phase shift errors in the measured data signal. In addition, the criterion for adjusting the calibration signal amplitude such that sidebands are below the system noise level no longer exists with the injection system. Table III lists the requirements for successful use of the injection system that uses a sine wave signal generator.

Table III: Requirements for successful calibration of the 13.3 GHz scatterometer using the injection system with sine wave input.

Parameter	Requirement
Calibration oscillator signal A_c	• k_2 accurately measured • A_c accurately measured • no variation in A_c
Modulator characteristics	• α_m accurately measured • no variations of α_m

Design 4 - Signal injection: square wave

This design uses the same method of injecting the calibration signal into the receiver Redop 1 channel with the exception that the modulation waveform is a saturating square-wave instead of a small sinusoid. Therefore, the block diagram of Figure 4 is applicable to this design. Again, the modulator can be either a ferrite device or a PIN diode with the latter offering an advantage in stability and reliability.

Appendix II presents the complete analysis of the use of the square-wave calibration signal in the design of Figure 4. The analysis consists of expanding the square wave as a Fourier series, then selecting the appropriate terms of the infinite series composed of all odd harmonics of the fundamental frequency. It will be shown in the following sketches of spectral response that this technique eliminates the dependency of the calibration signal on the amplitude of the output of the calibration signal generator as well as on the transfer 'gain' characteristic α_m of the modulator. In other words, the use of the square-wave modulation eliminates all the requirements specified in both Tables II and III (except the need to know k_2) and results in an ideal calibration method that is independent of all calibration system variables and is dependent only on the variables of net receiver gain and transmitter power.

Figure 7 shows the frequency spectrum plotted at the same points in the 13.3 GHz scatterometer system as those of Figure 5. Figure 7(a) shows the output spectrum of the calibrate-signal modulator. For this figure, it should be noted that the term α_M is the maximum gain of the modulator and is not equal to α_m used previously as the transfer 'gain' characteristic of the modulator. Also note from the figure that the calibration signal amplitude at frequencies ($\omega_o \pm \omega_c$) is independent of the calibration signal generator amplitude. This is because the square wave is adjusted such that there is either maximum gain

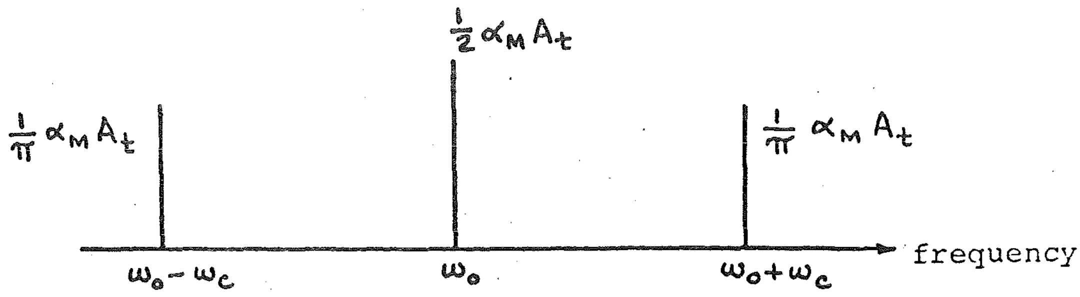

(a) Spectrum at the output of the calibrate signal modulator.

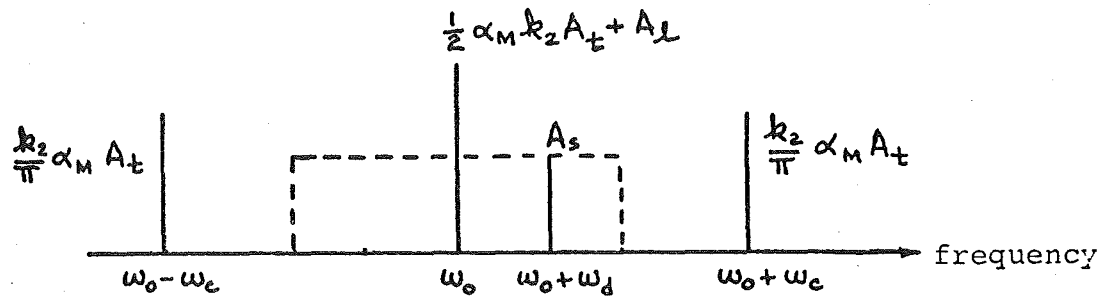

(b) Spectrum at the input to the mixer.

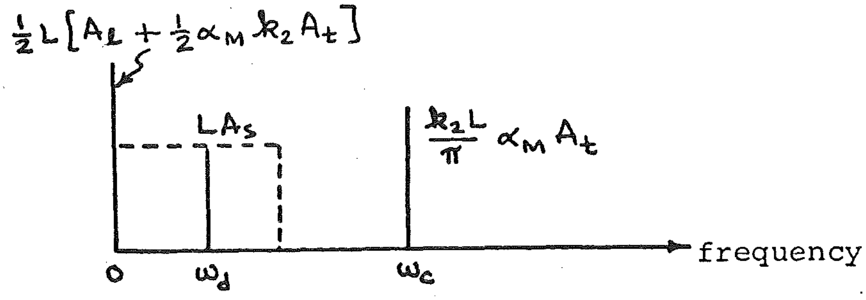

(c) Spectrum at the output of the mixer.

Figure 7: Frequency spectrum in 13.3 GHz scatterometer using signal injection method for calibration. A square wave is used as the calibration signal source.

α_M or minimum gain (~ 0) through the device. Since these are fixed constants unique to the device, the only variable in the spectral terms of Figure 7(a) is A_t, the transmitter sample.

Figure 8 below shows the output spectrum of the 13.3 GHz scatterometer using the injection calibration technique together with square-wave signal modulation. From the figure, the calibration signal at the output of the scatterometer is that given in equation (10).

$$y_c(t) = \frac{1}{\pi} \alpha_M k_2 LGA_t \cos \omega_c t \tag{10}$$

where: α_M = maximum gain of the modulator.

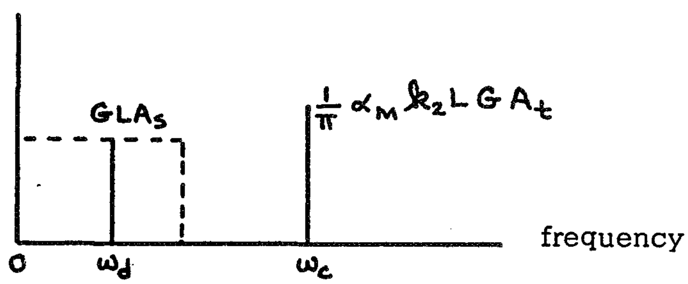

Figure 8: Output spectrum of the 13.3 GHz scatterometer with square-wave calibration signal injection.

Equation (10) shows that a definite advantage has been realized by using a square-wave as the modulation waveform. The calibration signal at the output of the scatterometer is independent of the calibration circuitry (with the exception that the minimum and maximum attenuation of the modulator and the directional coupler factors must be known constants) and is dependent only upon the scatterometer variables which are to be calibrated (LGA_t). Therefore, the square-wave injection system is the ideal calibration method for use with the 13.3 GHz scatterometer and it is herein recommended that the present equipment be modified to use this technique.

When using the square-wave injection system, a question arises concerning the relation between square-wave distortion and the resulting calibration signal error. Note II in Appendix IV contains an analysis of this relationship where it is assumed that the leading and trailing edges of the square wave have a sinusoidal shape. This can be considered to be a 'worst case' condition because the non-ideal leading and trailing edge response at the fundamental frequency of the square wave will result in the maximum change in the calibration signal. Thus, this analysis presents an upper-bound on distortion of the square wave.

If one assumes a square wave whose amplitude varies from zero to A_o then it can be shown (as in Appendix II) that, for a calibration signal error of less than 0.4%, the rise time must be less than or equal to 0.016 G, where T is the period of the calibration signal. For example, if the frequency of the calibrate signal is 10 kHz, then $T = 10^{-4}$ seconds and the maximum rise time of the square-wave (for less than 0.4% calibration error) is 1.6 microseconds.

Conclusions

An analysis has been presented of four methods available for dynamic calibration of the 13.3 GHz scatterometer system. A detailed mathematical treatment has been given for each method with the requirements listed for acceptable use of the method.

The present calibration system was shown to be unacceptable because of the dependency of the calibration signal on variables within the calibration system itself. These variables include the calibration oscillator amplitude, the ferrite modulator attenuation characteristic and the transmitter-to-receiver leakage power. The bias point of the ferrite modulator is dependent upon residual magnetization of the ferrite material. Any change in this operating point due to either internal or external influences will change the calibration signal amplitude. In addition, phase and amplitude characteristics of the ferrite modulator in the data signal path lead to error in the separation of fore and aft information. Because these variations cannot be monitored, the bias level of measured scattering coefficient data is variable at the same time that accuracy of the relative data is variable due to phase and amplitude variations of the ferrite modulator.

The second calibration method considered in the analysis simply replaces the ferrite modulator in the present system by a solid-state PIN diode modulator. The only advantage of this method compared to the present method is in the increased stability of the modulation device. Because the variations in the calibration signal can still occur, this method is equally unacceptable for calibrating the 13.3 GHz scatterometer.

The third and fourth designs inject a sample of the transmit signal offset by the calibration signal frequency into the receive rf signal path. The advantage of this technique compared to designs one and two is that there is no active device in the rf signal path but simply an rf directional coupler. Therefore, phase and amplitude errors in the data due to the calibration system are eliminated using this technique. In design three, a sinusoidal signal is used to modulate the transmitter sample before it is injected into the receive channel. The calibration signal thus produced remains dependent upon the modulator characteristic and the calibration oscillator amplitude. Because these parameters are both subject to variation, this design is undesirable.

The fourth design uses a square-wave signal to modulate the transmitter sample preceding injecting into the receiver rf circuitry. This method has the advantage that the calibration signal recorded on the data tape recorder is dependent only upon the transmitter sample and the net receiver gain, the parameters which are to be monitored by the calibration signal. Because this signal is independent of calibration system variables and data errors are minimized by removing the active modulator from the receiver rf circuitry, this design can be considered ideal for use with the 13.3 GHz scatterometer.

It is recommended that the 13.3 GHz scatterometer be modified to include the fourth calibration design. Further, it is recommended that a PIN diode modulator be used in the calibration circuitry because of the advantage of increased stability and reliability afforded by this device compared to a ferrite modulator. The major modification in the equipment will be in the microwave circuitry with the modulator removed from the rf signal line and additional circuitry added to achieve the calibration injection. Comparison of Figures 1 and 4 indicates the extent of these modifications. In addition, the calibration oscillator must be replaced with a square-wave generator.

It is expected that modification of the calibration circuitry to that recommended in this paper will result in a major improvement in the accuracy of data measured by the 13.3 GHz scatterometer. Further, the consistency of the quality of these data measurements when comparing separate missions will be established which will allow precise conclusions to be reached regarding the behavior of the scattering coefficient in relation to terrain characteristics. Because this is the objective of the aircraft testing scatterometry program, it is required that the recommended modification be incorporated into the equipment as soon as possible.

APPENDIX I

ANALYSIS OF PRESENT CALIBRATION SYSTEM

APPENDIX I: Analysis of present calibration system.

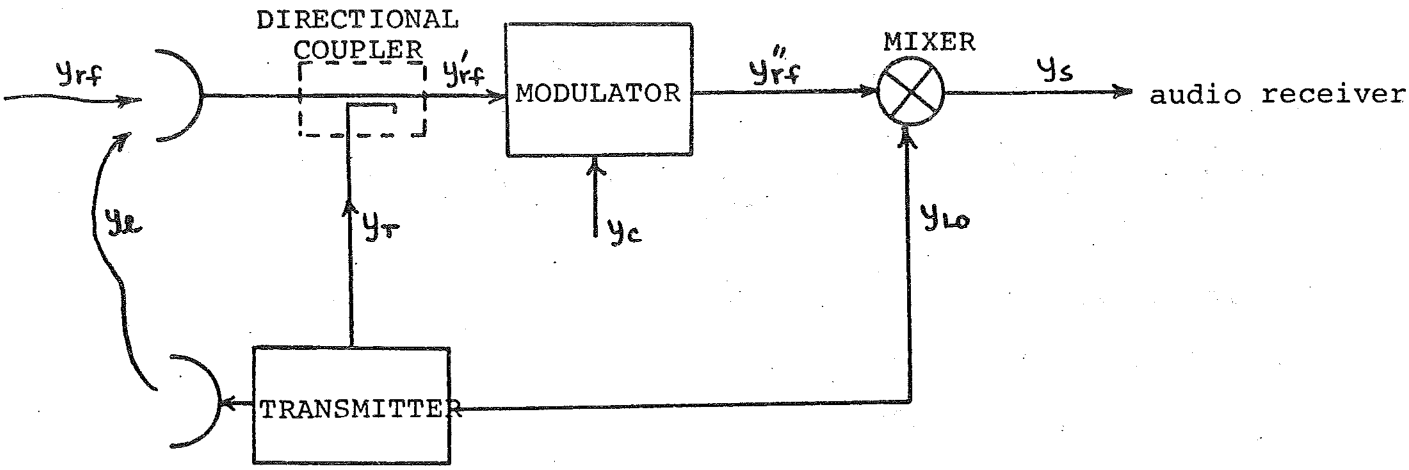

Let:

$$y_{rf} = A_s \cos(\omega_o + \omega_d)t$$

$$y_\ell = A_\ell \cos \omega_o t$$

$$y_T = A_t \cos \omega_o t$$

$$y_c = A_c \cos \omega_c t$$

$$y_{LO} = A_{LO} \cos \omega_o t$$

Consider first the return data signal y_{rf} :

$$y_{rf} = A_s \cos(\omega_o + \omega_d)t \qquad \text{(I-1)}$$

where: A_s = amplitude of signal at frequency $(\omega_o+\omega_d)$, in volts

ω_o = carrier frequency, in radians/second

ω_d = Doppler frequency corresponding to incident angle Θ, in radians/second

The frequency spectrum of y_{rf} is shown below

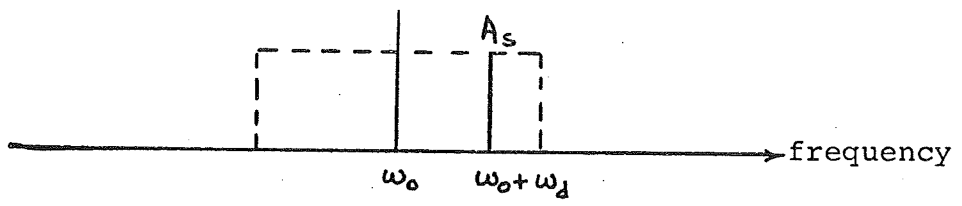

The signal y'_{rf} is modified from y_{rf} by coupling an attenuated sample of the transmitter energy at frequency ω_o into the spectrum of y_{rf}. In addition, a small amount of transmit energy enters the receiver through antenna coupling.

$$y'_{rf} = y_{rf} + y_T + y_\ell$$

$$= A_s \cos(\omega_o + \omega_d)t + A_t \cos \omega_o t + A_\ell \cos \omega_o t$$

$$y'_{rf} = A_s \cos(\omega_o + \omega_d)t + A_x \cos \omega_o t \qquad (\text{I-2})$$

where: $A_x = A_t + A_\ell$

A_t = amplitude of coupled transmit sample

A_ℓ = amplitude of leakage signal

The frequency spectrum of y'_{rf} is shown below

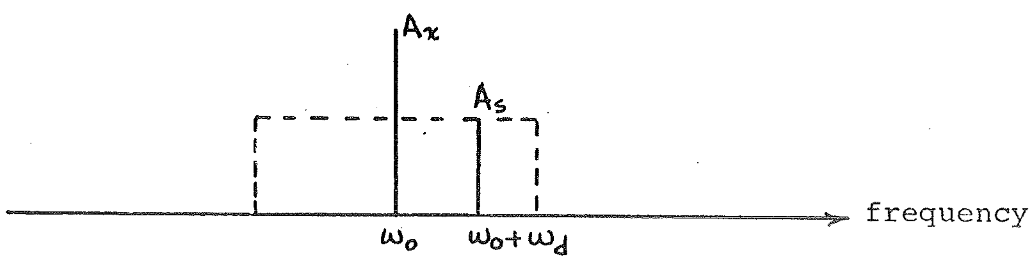

The signal y'_{rf} is now transferred through the ferrite modulator which, in combination with the transmit sample A_x, causes the calibration signal y_c to be generated in the receiver frequency spectrum. As an aside, let us consider the operation of the ferrite modulator.

The ferrite modulator operates as a variable isolator with the amount of Faraday rotation, and hence, the amount of isolation, controlled by the modulating signal. Representing the device as shown below, we can derive the transfer equation which we will use to modify y'_{rf}.

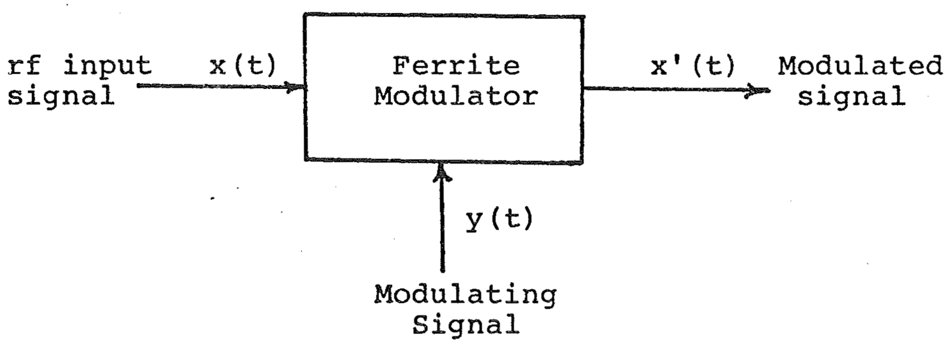

The output signal from the modulator is given by the following expression (assuming operation at an appropriate bias point α_o)

$$x'(t) = (\alpha_o - \alpha_m y(t))\, x(t) \qquad \text{(I-3)}$$

where: α_o = quiescent 'gain' with $y(t) = 0$

α_m = transfer 'gain' characteristic of the ferrite modulator

The signal y''_{rf} can now be written by using equations (I-2) and (I-3).

$$y''_{rf} = (\alpha_o - \alpha_m A_c \cos\omega_c t)\left[A_s \cos(\omega_o+\omega_d)t + A_x \cos\omega_o t\right] \tag{I-4}$$

Then, expanding and using the appropriate trigonometric relations, equation (I-4) becomes

$$\begin{aligned} y''_{rf} = {} & \alpha_o\left[A_x \cos\omega_o t + A_s \cos(\omega_o+\omega_d)t\right] \\ & - \alpha_m\left[\frac{A_c A_x}{2}\cos(\omega_o+\omega_c)t + \frac{A_c A_x}{2}\cos(\omega_o-\omega_c)t\right] \\ & - \alpha_m\left[\frac{A_c A_s}{2}\cos(\omega_o+\omega_c+\omega_d)t + \frac{A_c A_s}{2}\cos(\omega_o-\omega_c+\omega_d)t\right] \end{aligned} \tag{I-5}$$

The frequency spectrum of equation (I-5) is shown in the figure below.

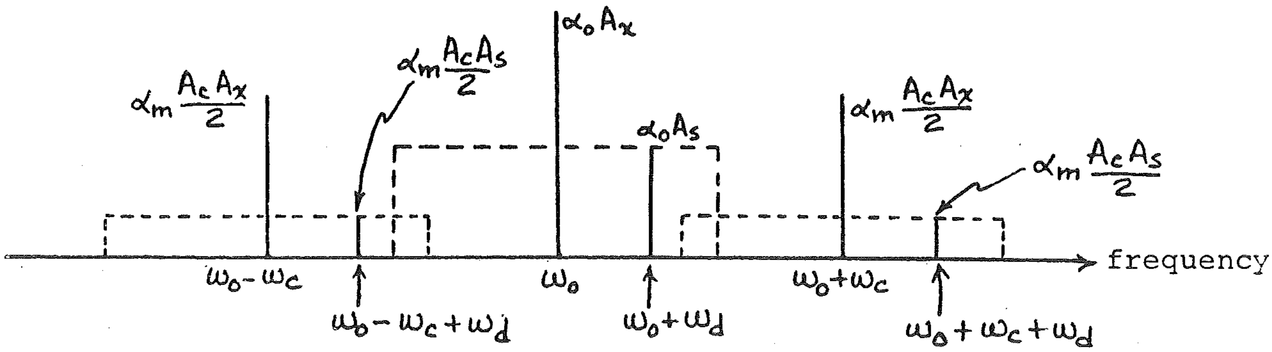

Consider now the mixing operation. The notation we shall use to describe the operation is shown in the figure below.

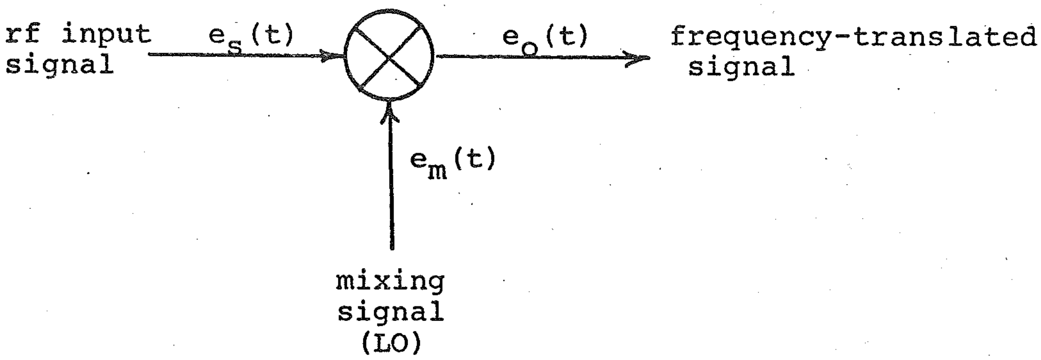

$$e_s(t) = E_s \cos \omega_s t$$
$$e_m(t) = E_m \cos \omega_o t$$

If $E_m \gg E_s$, then the output signal $e_o(t)$ will have the following form.

$$e_o(t) = k_o e_s + k_1 e_m + L e_s \cos \omega_o t \qquad \text{(I-6)}$$

where: k_o, k_1 = mixing constants

L = mixing gain at sideband frequencies

It should be noted in equation (I-6) that the sideband amplitudes located at frequencies $(\omega_o \pm \omega_s)$ are dependent only on the signal amplitude and mixing gain and are independent of the magnitude of the mixing signal amplitude E_m. This is for the case where $E_m \gg E_s$ which is the typical case for mixing operations.

Now, applying the results of equation (I-6) to signal y''_{rf} given in equation (I-5), we arrive at the audio scatterometer signal $y_s(t)$.

$$y_s(t) = k_0 y''_{rf} + k_1 A_{LO} \cos \omega_o t + L y''_{rf} \cos \omega_o t \tag{I-7}$$

Clearly, we are interested only in the last term since all other terms of equation (I-7) appear at frequencies out of the audio band. Substituting equation (I-5) in (I-7), $y_s(t)$ becomes the following.

$$\begin{aligned} y_s(t) = {} & \tfrac{1}{2}\alpha_o L A_x + \tfrac{1}{2}\alpha_o L A_s \cos \omega_d t \\ & - \tfrac{1}{4}\alpha_m L A_c A_x \cos \omega_c t - \tfrac{1}{4}\alpha_m L A_c A_x \cos(-\omega_c)t \\ & - \tfrac{1}{4}\alpha_m L A_c A_s \cos(\omega_c + \omega_d)t - \tfrac{1}{4}\alpha_m L A_c A_s \cos(-\omega_c + \omega_d)t \end{aligned} \tag{I-8}$$

From the mixer analysis, the calibrate signal at frequency ω_c is independent of the local oscillator amplitude A_{lo} if $A_{LO} \gg \alpha_m \frac{A_c A_x}{2}$. From equation (I-8), we can see the folding operation that occurs when mixing the carrier frequency down to dc. Thus, $\cos(-\omega_c)t$ is translated to $\cos \omega_c t$ and $\cos(-\omega_c + \omega_d)t$ to $\cos(\omega_c - \omega_d)t$. The spectral plot below illustrates this for the case where fore and aft signals (at $+\omega_d$ and $-\omega_d$, respectively) are equal.

Unfolded spectrum:

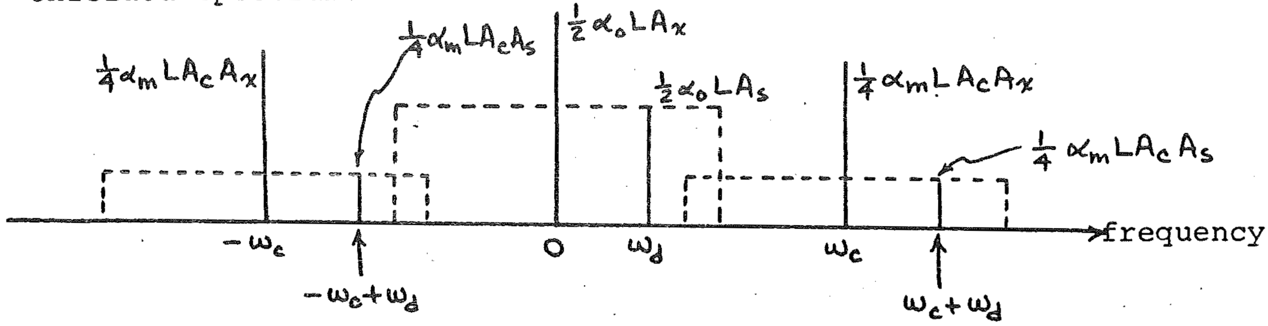

Folded spectrum:

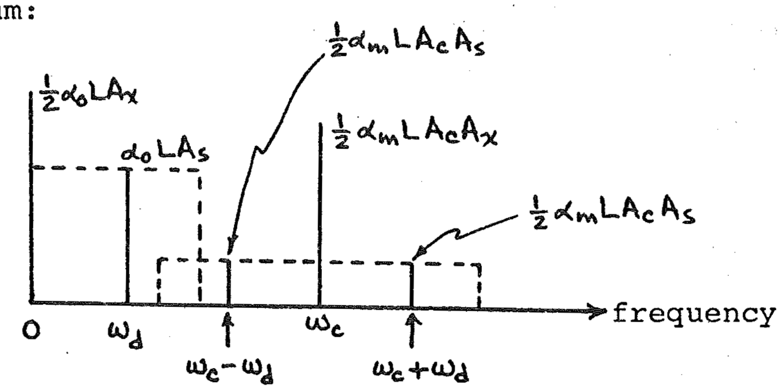

Consider the spectrum of the data signal about the calibrate signal at frequency ω_c. The ratio of the signal at ω_c to that at $\omega_c \pm \omega_d$ is

$$\frac{\frac{1}{2}\alpha_m L A_c A_x}{\frac{1}{2}\alpha_m L A_c A_s} = \frac{A_x}{A_s}$$

Therefore, if $A_x \gg A_s$ and if A_c is adjusted such that

$$\frac{1}{2}\alpha_m L A_c A_s < N$$

where: N is the system rms noise floor at audio,

then the interaction between data and calibrate signal will not appear in the spectrum. This is shown in the figure below.

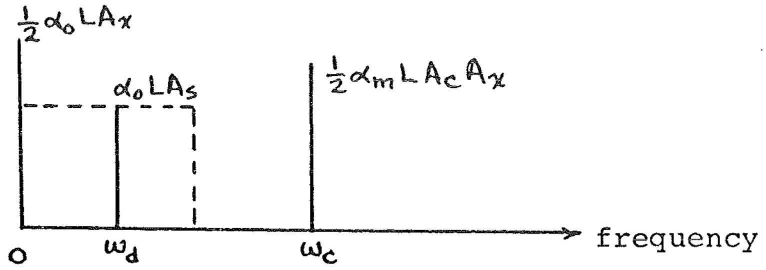

The conditions for correct operation of this calibration system are summarized below.

(1) appropriate bias level (see Appendix IV, Note 1)

(2) at the coupler, $A_x \gg A_s$

(3) at the ferrite modulator, $A_c < \dfrac{2N}{\alpha_m L A_s}$

(4) at the mixer, $A_{lo} \gg \alpha_m \dfrac{A_c A_x}{2}$

where: A_x = total transmitter sample (coupled + leakage) at the input to the ferrite modulator

A_s = received signal amplitude

A_c = calibrate signal amplitude

A_{lo} = local oscillator signal amplitude

N = noise floor at audio

α_m = transfer 'gain' characteristic of modulator

L = mixer sideband gain

APPENDIX II

ANALYSIS OF INJECTION CALIBRATION SYSTEM

APPENDIX II: Analysis of Injection Calibration System.

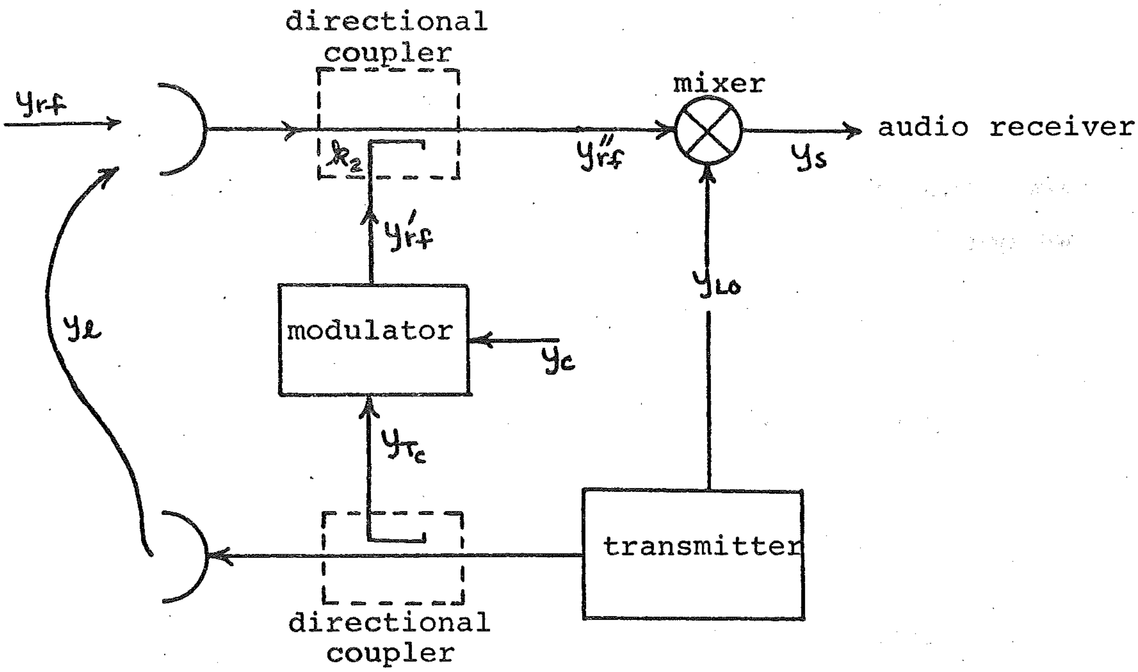

Let:

$$y_{rf} = A_s \cos(\omega_o + \omega_d)t$$

$$y_\ell = A_\ell \cos \omega_o t$$

$$y_{T_c} = A_t \cos \omega_o t$$

$$y_c = F_c(t)$$

$$y_{LO} = A_{LO} \cos \omega_o t$$

Consider first the rf signal y'_{rf} which is the transmitter signal y_{T_C} modified by the calibrate signal y_C. We shall treat the transfer function of the modulator in an analogous way to that used in Appendix I (i.e. as a variable 'gain' device). Then, rewriting equation (I-3) in our present notation, we get the following expression.

$$y'_{rf} = (\alpha_o - \alpha_m y_c(t))\, y_{T_c}$$

where: α_o = modulator quiescent gain with $y_c(t) = 0$

α_m = gain transfer characteristic of the modulator

Now, substituting the appropriate expressions for $y_c(t)$ and $y_{T_C}(t)$, we get

$$y'_{rf} = (\alpha_o - \alpha_m F_c(t))\, A_t \cos \omega_o t \qquad \text{(II-1)}$$

A. <u>Injection system with calibration signal sinusoidal.</u>

Let $F_c(t) = A_c \cos \omega_c t$

Equation (II-1) then becomes

$$y'_{rf} = \alpha_o A_t \cos \omega_o t - \tfrac{1}{2}\alpha_m A_c A_t \cos(\omega_o + \omega_c)t$$
$$- \tfrac{1}{2}\alpha_m A_c A_t \cos(\omega_o - \omega_c)t \qquad \text{(II-2)}$$

The spectrum of this signal is shown in the figure below.

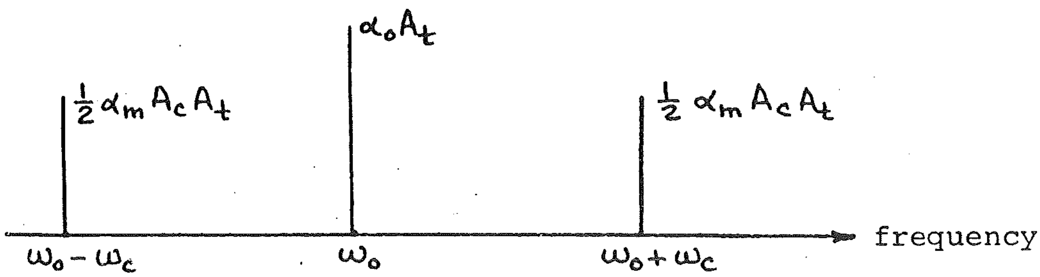

The signal at the output of the directional coupler y''_{rf} can now be found as follows.

$$y''_{rf} = y_{rf} + y_{\ell} + y'_{rf} k_2$$

or

$$\begin{aligned} y''_{rf} = {} & A_s \cos(\omega_o + \omega_d)t + A_{\ell} \cos \omega_o t \\ & + \alpha_o k_2 A_t \cos \omega_o t - \tfrac{1}{2}\alpha_m k_2 A_c A_t \cos(\omega_o + \omega_c)t \\ & - \tfrac{1}{2}\alpha_m k_2 A_c A_t \cos(\omega_o - \omega_c)t \end{aligned} \qquad \text{(II-3)}$$

where: k_2 = coupling coefficient of the directional coupler.

The spectrum of y''_{rf} is shown in the figure below.

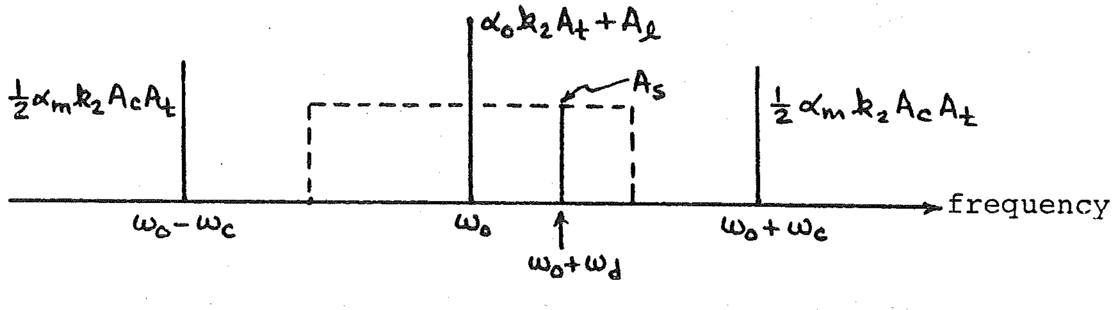

Now, using equation (I-7) from Appendix I, the signal y_s at the output of the mixer is

$$y_s(t) = L\, y''_{rf} \cos \omega_o t \ + \text{ higher frequency terms}$$

where: L = mixing gain at sideband frequencies

$A_{lo} >> A_s$.

Then,

$$y_s = \frac{1}{2} L (\alpha_o k_2 A_t + A_\ell) + \frac{1}{2} L A_s \cos \omega_d t$$
$$- \frac{1}{4} \alpha_m k_2 L A_c A_t \cos \omega_c t - \frac{1}{4} \alpha_m k_2 L A_c A_t \cos (-\omega_c) t$$

or

$$y_s = \frac{1}{2} L (\alpha_o k_2 A_t + A_\ell) + \frac{1}{2} L A_s \cos \omega_d t$$
$$- \frac{1}{2} \alpha_m k_2 L A_c A_t \cos \omega_c t \qquad \text{(II-4)}$$

Again, if we assume that data signals at negative Doppler frequencies are equal to those at positive Doppler frequencies, then the frequency spectrum of y_s will appear as shown below.

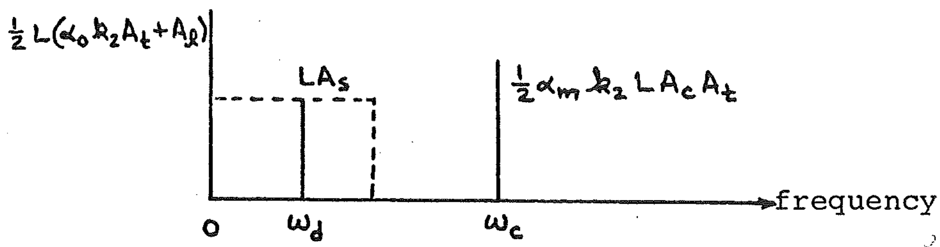

Clearly, this method has the following advantages compared to the present method analyzed in Appendix I:

1. Data signal not subjected to insertion loss and phase shift of modulator.

2. Calibration signal independent of the transmitter leakage power.

The principal disadvantage is the dependence of the calibration signal at audio on the amplitude of the calibrate oscillator

B. Injection system with square wave calibration signal.

Consider the square wave sketched in the figure below.

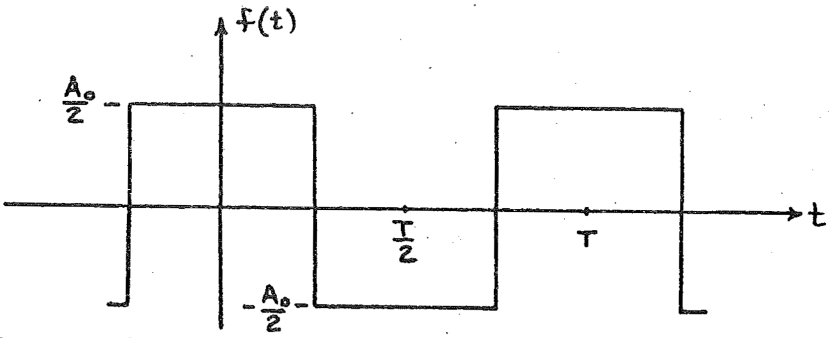

The Fourier series expansion for f(t) is

$$f(t) = \frac{a_o}{2} + \sum_{n=1}^{\infty} a_n \cos n\omega t + \sum_{n=1}^{\infty} b_n \sin n\omega t$$

where:

$$a_n = \frac{2}{T}\int_0^T f(t) \cos n\omega t \, dt \quad ; \quad b_n = 0 \qquad \text{(even function)}$$

Calculating the coefficients, f(t) becomes

$$f(t) = \frac{2A_o}{\pi}\left[\cos \omega_c t - \frac{1}{3}\cos 3\omega_c t + \frac{1}{5}\cos 5\omega_c t - \ldots\right] \tag{II-5}$$

where: ω_c = the calibrate signal frequency

Referring to equation (II-5), the only term we need consider for use in the calibration system is that appearing at frequency ω_c. The remaining terms will appear outside the audio bandwidth at the output of the scatterometer. Thus, if the calibrate frequency is 10 kHz, the higher-order terms of (II-5) will be at 30 kHz, 50 kHz etc sufficiently outside the audio bandwidth.

Applying the results of the Fourier expansion of the square wave, the signal $F_c(t)$ in equation (II-1) will be

$$F_c(t) = \frac{2A_o}{\pi} \cos \omega_c t$$

Suppose that the peak-to-peak amplitude of the square wave A_o corresponds to the net difference between maximum gain α_M and minimum gain (assumed zero) of the modulator. Then

$$\alpha_m F_c(t) = \frac{2\alpha_M}{\pi} \cos \omega_c t$$

where: α_M = maximum 'gain' of the modulator

α_m = transfer'gain' characteristic of the modulator

Substituting this expression in equation (II-1) results in the expression for the calibration signal at rf preceding injection into the receive data spectrum. We note that, since the modulator will operate between minimum and maximum 'gain', the modulator bias α_o will be adjusted to $\frac{1}{2}\alpha_M$. Then

$$y'_{rf} = (\alpha_o - \alpha_m F_c(t)) A_t \cos \omega_o t$$

$$= \alpha_M \left(\frac{1}{2} - \frac{2}{\pi} \cos \omega_c t\right) A_t \cos \omega_o t$$

Expanding the trigonometric quantities results in the following expression.

$$y'_{rf} = \frac{1}{2}\alpha_M A_t \cos \omega_o t - \frac{1}{\pi}\alpha_M A_t \cos(\omega_o + \omega_c)t$$

$$- \frac{1}{\pi}\alpha_M A_t \cos(\omega_o - \omega_c)t \qquad \text{(II-6)}$$

The frequency spectrum of y'_{rf} is shown below.

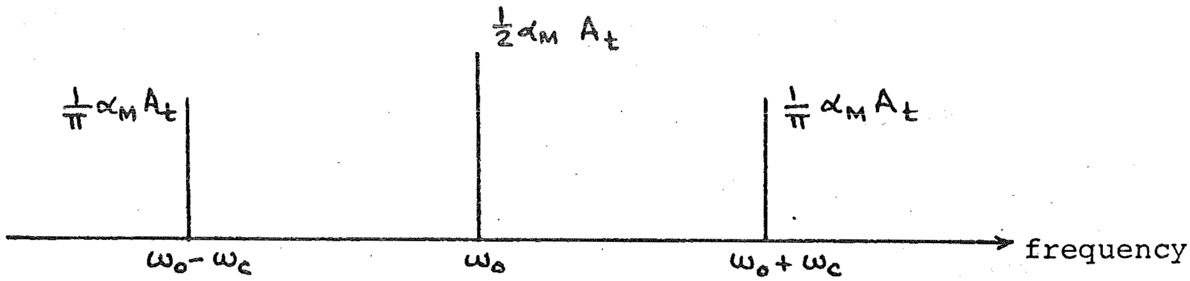

Following the analysis developed for the sinusoidal calibrate signal, we compute the combined signal at the output of the directional coupler y''_{rf}.

$$y''_{rf} = y_{rf} + y_\ell + y'_{rf} k_2$$

or

$$y''_{rf} = A_s \cos(\omega_o + \omega_d)t + A_\ell \cos \omega_o t + \frac{1}{2}\alpha_M k_2 A_t \cos \omega_o t - \frac{k_2}{\pi}\alpha_M A_t \cos(\omega_o + \omega_c)t - \frac{k_2}{\pi}\alpha_M A_t \cos(\omega_o - \omega_c)t \qquad \text{(II-7)}$$

The frequency spectrum of y''_{rf} is shown in the figure below.

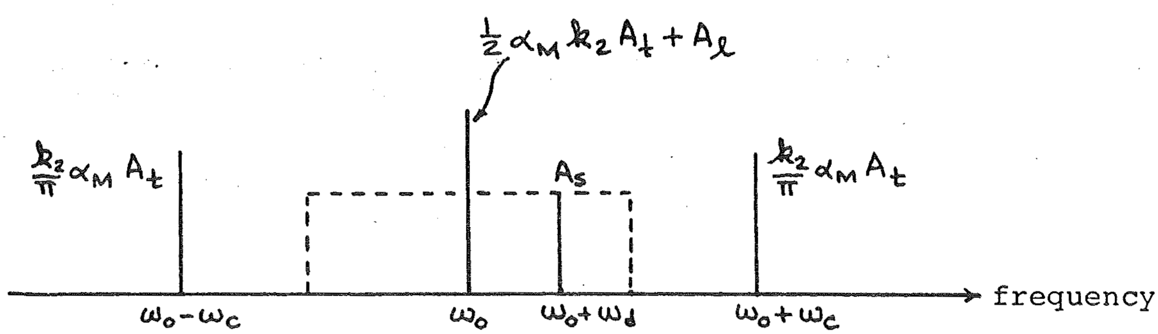

Again using equation (I-7) from Appendix I, the signal y_s at the output of the mixer is

$$y_s = L\, y''_{rf} \cos \omega_o t + \text{higher frequency terms}$$

where: L = mixing gain at sideband frequencies

$A_{lo} \gg A_s$

Then

$$y_s = \tfrac{1}{2} L \left[A_\ell + \tfrac{1}{2} \alpha_M k_2 A_t \right] + \tfrac{1}{2} L A_s \cos \omega_d t - L \frac{k_2}{\pi} \alpha_M A_t \cos \omega_c t \qquad \text{(II-8)}$$

Assuming equal positive and negative Doppler data signals, the spectrum at the output of the mixer is shown in the figure below.

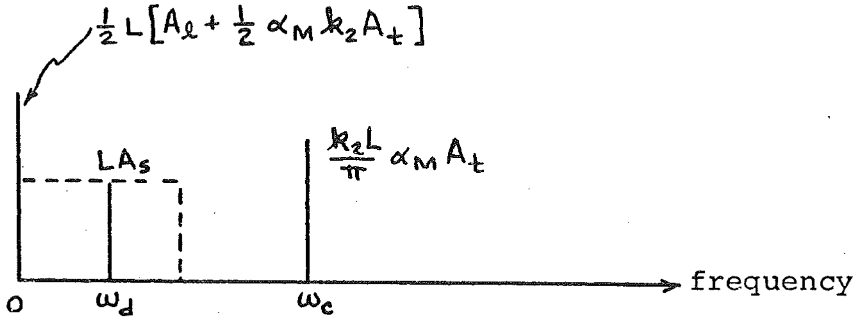

Advantages of square-wave calibration injection system:

1. Data signal independent of insertion loss and phase shift of modulator.

2. Calibrate signal independent of transmitter leakage.

3. Calibrate signal at preamp input dependent only on transmitter level A_t ($\frac{1}{\pi} k_2 L \alpha_M \equiv$ fixed constant)

APPENDIX III

THE PIN DIODE MODULATOR

APPENDIX III: The PIN Diode Modulator by Rod L. Angle

A. Physical and Mathematical Description.

The PIN diode is made up of three layers of semiconductor material. The middle layer is an intrinsic (I) region sandwiched between a P-type layer and an N-type layer. The diode at low frequencies acts as an ordinary rectifying diode; but acts as a pure resistance at high frequencies due to the charge storage capabilities of the I region. The transition, or 'changeover', frequency that separates these two characteristics is defined as f_o where

$$f_o = \frac{1}{2\pi\tau}$$

where: τ = recombination lifetime in the I region

Thus, at frequencies below f_o, the diode is a normal diode and above f_o, the diode is a resistor. The recombination lifetime τ is a controlled parameter usually between 0.03 microseconds and 3 microseconds. Taking a typical value τ = 0.1 microseconds, f_o = 1.6 MHz. Therefore, for an application of the PIN diode as a modulator at 13.3 GHz, the diode can be considered as a pure resistance.

The conduction of the PIN diode is proportional to the stored charge which, in turn, is proportional to the diode current given in the following expression.

$$i_d = \frac{dQ_d}{dt} + \frac{Q_d}{\tau}$$

where: i_d = diode current

Q_d = charge stored in the diode

Now, if the diode is biased by a dc current, then

$$Q_d = \tau I_d$$

where: I_d = dc bias current

Because the resistance of the device is proportional to the charge stored Q_d, the resistance can be controlled by the dc bias current I_d. It should be noted that Q_d, and hence the resistance, is independent of the rf current for sufficiently high frequencies.

A device with these characteristics can clearly be used as an rf modulator in either a pulse or an amplitude modulator circuit. Although the resistance vs current characteristic of the PIN diode is nearly linear, the preferred application would use a square wave or a pulse as the modulating waveform.

B. Advantages of using the PIN diode modulator.

The PIN diode absorbs power with the microwave energy dissipated as heat. This tends to eliminate reflections together with associated VSWR problems in the rf microwave circuitry. As long as the rf power through the diode is below one watt, the dissipation will not exceed the limits of the device and harmonic distortion will be minimized. Since the diode resistance change (controlled by the calibration signal) is operated at a much lower frequency than the rf signal, the interaction between the klystron frequency and the modulator will be minimal. Perhaps most importantly for the 13.3 GHz scatterometer application, the temperature dependence of the PIN diode modulator can be kept to a minimum by using a temperature sensitive element in the bias source. Thus, by simply changing the bias point of the diode, we can compensate for any temperature variations.

In the usual circuit configuration, the PIN diode modulator contains more than one diode. This increases the attenuation capabilities but more importantly, has the advantage of reducing the reflection caused by the presence of the single diode. With the diodes spaced a quarter-wavelength apart, this reflection can be reduced to a minimum.

The principal advantages of the PIN diode modulator are listed below.

1. The PIN diode modulator driven by a square wave will not introduce any extraneous spectral impurities due to the non-linearity of the diode characteristic as it would with a sinusoidal waveform.

2. Errors in matching and reflections during switching are minimal for a PIN diode modulator.

3. Parasitic resistances exist in the diode and its circuitry which affect the attenuation. However, with proper biasing, these parasitics can be reduced to provide operation independent of the parasitics of the configuration

4. By proper package design and placement in the waveguide, the insertion loss can be minimized and the isolation can be maximized.

C. The PIN diode in a square-wave modulator.

1. The PIN diode resistance vs. dc bias current.

The figure below is from Hewlett-Packard Applications Note AN-922. This represents a typical PIN diode with the exact values dependent upon the particular diode chosen.

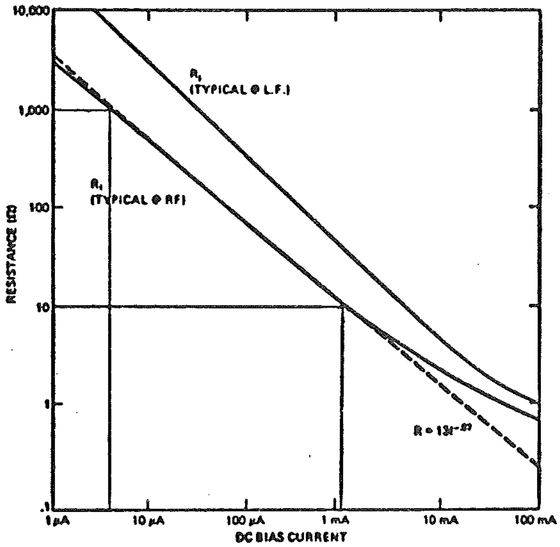

Figure III-1. Resistance of a PIN diode vs. bias current.

2. Circuit representation of the PIN diode modulator.

The PIN diode modulator can be considered as a variable load resistance in parallel with the rf signal. As the resistance changes, so does the amplitude of the rf signal appearing at the output terminals. The equivalent circuit is shown in the figure below.

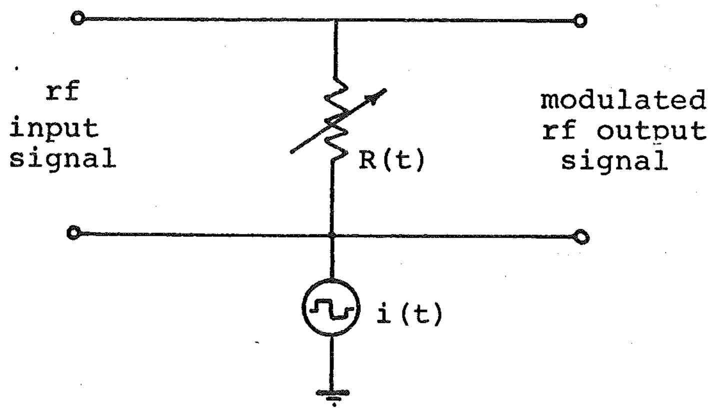

Figure III-2. Equivalent circuit of PIN diode modulator.

The rf input signal is at a frequency of 13.3 GHz and is a sample of the output of the transmitter. The current bias i(t) is a square wave with a typical maximum value of 1 milliampere and a minimum value of 5 microampere. From Figure III-1, this range of i(t) gives a typical resistance range of 10 ohms to 1000 ohms. If the impedance seen at the output is 500 ohms, then the 'gain'

G(t) of the circuit will have a maximum of 0.667 at R(t) = 1000 ohms and a minimum of zero at R(t) = 10 ohms. The figures appearing below illustrate this relationship.

Bias current i(t)

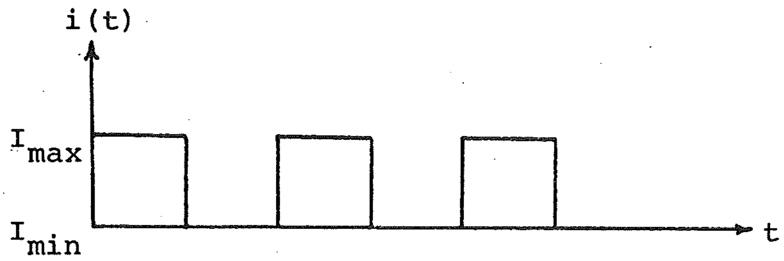

PIN diode resistance R(t)

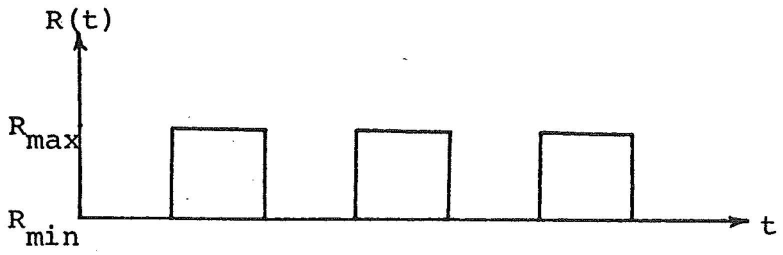

Circuit Gain G(t) (Z_o = 50 ohms)

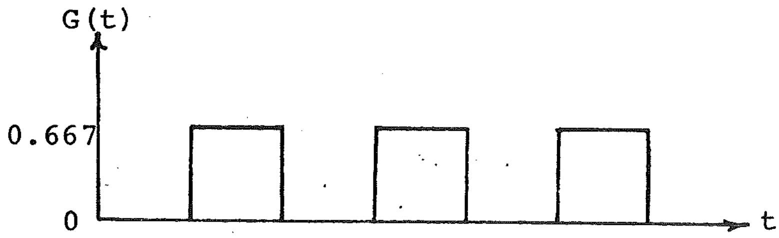

APPENDIX IV

ANALYSIS OF MICROWAVE MODULATORS

APPENDIX IV: Analysis of Microwave Modulators.

NOTE I. On the use of variable attenuators as modulators.

A. Ferrite modulator using sinusoidal modulating signal.

The transfer 'gain' of the ferrite modulator plotted as a function of the solenoid field z(t) is shown in the figure below. Note that the maximum gain α_M occurs when z(t) = 0 and the gain response is symmetrical about the z(t) = 0 axis. The slope of the response is α_m with the bias or quiescent point located at α_o. The bias point is established in the present system configuration by the remanent magnetism of the ferrite material. The purpose of this note is to compute the amplitude of the calibration signal as a function of the location of the bias point as well as the transfer slope of the 'gain'.

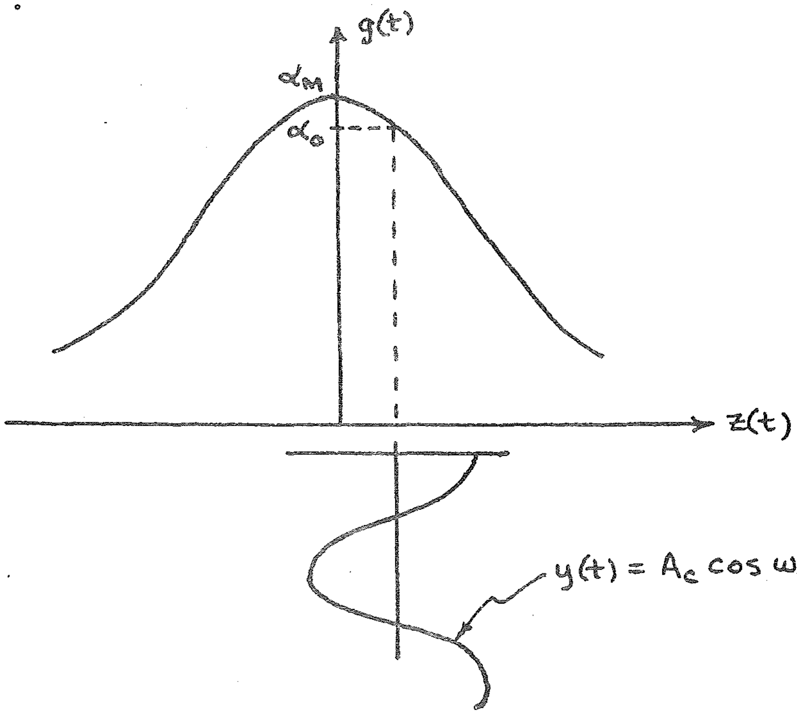

Transfer 'gain' response of the ferrite modulator.

The modulation waveform can be plotted from the above figure using the characteristics of the 'gain' response in combination with the modulating signal y(t). This is shown in the figure below for the general case where a portion of the operating region occurs about the origin of the 'gain' response. From the figure it can be seen that the location of the bias point α_o will determine the harmonic content of the modulated spectrum and will directly influence the amplitude of the calibration signal. Thus, if α_o coincides with α_M, the maximum 'gain', then the modulation sidebands will appear at frequencies $\pm 2\omega_c$ about the carrier frequency ω_o. In contrast, the desired operation is when α_o is such that the signal y(t) operates completely in the first quadrant of the 'gain' characteristic and, in addition, in a linear region of the response. For this case, modulation sidebands will occur at frequencies $\pm \omega_c$ about the carrier frequency and will represent the desired calibration signal.

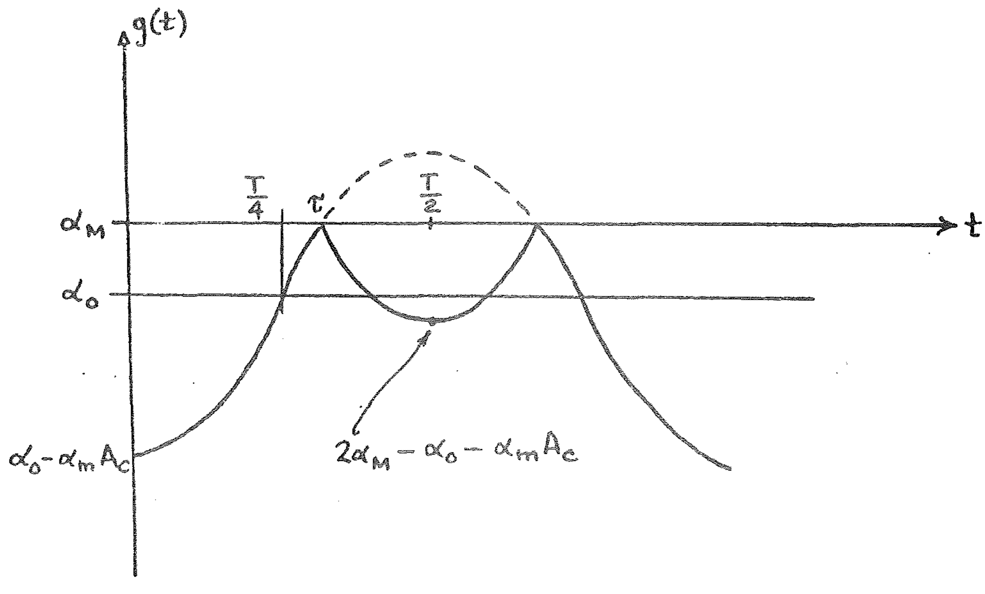

Modulation waveform of the ferrite modulator.

The variable 'gain' in the above figure can be expressed analytically in a Fourier series as follows.

$$g(t) = \frac{a_o}{2} + \sum_{n=1}^{\infty} a_n \cos n\omega t \qquad \text{(N1-1)}$$

where:

$$a_n = \frac{4}{T}\int_0^{T/2} f(t) \cos n\omega t \, dt$$

$$T = \text{period of } y(t) = \frac{2\pi}{\omega_c}$$

The function f(t) can be determined from the figure by considering two regions separated by time τ. Thus, assuming constant slope α_m

$$f(t) = \alpha_o - \alpha_m A_c \cos \omega_c t \qquad o \le t \le \tau$$

$$f(t) = 2\alpha_M - \alpha_o + \alpha_m A_c \cos \omega_c t \qquad \tau \le t \le \frac{T}{2}$$

and at time $t = \tau$,

$$f(\tau) = \alpha_M$$

or

$$\cos \omega_c \tau = \frac{\alpha_o - \alpha_M}{\alpha_m A_c}, \quad \tau \le \frac{T}{2} \qquad \text{(N1-2)}$$

The coefficients for the Fourier expansion then become

$$a_n = \frac{4\alpha_o}{T}\int_0^{\tau} \cos n\omega_c t \, dt - \frac{4\alpha_m A_c}{T}\int_0^{\tau} \cos \omega_c t \cos n\omega_c t \, dt$$

$$+ \frac{4}{T}(2\alpha_M - \alpha_o)\int_{\tau}^{T/2} \cos n\omega_c t \, dt + \frac{4\alpha_m A_c}{T}\int_{\tau}^{T/2} \cos \omega_c t \cos n\omega_c t \, dt$$

The first three coefficients are listed below.

$$a_0 = \frac{8\tau}{T}(\alpha_0 - \alpha_M) + 2(2\alpha_M - \alpha_0) - \frac{4}{\pi}\alpha_m A_c \sin\omega_c\tau$$

$$a_1 = \alpha_m A_c \left(1 - \frac{4\tau}{T}\right) + \frac{4}{\pi}(\alpha_0 - \alpha_M)\sin\omega_c\tau$$

$$- \frac{2}{\pi}\alpha_m A_c \sin\omega_c\tau \cos\omega_c\tau \qquad \text{(N1-3)}$$

$$a_2 = \frac{2}{\pi}(\alpha_0 - \alpha_M)\sin 2\omega_c\tau - \frac{2}{\pi}\alpha_m A_c \sin\omega_c\tau$$

$$- \frac{2}{3\pi}\alpha_m A_c \sin 3\omega_c\tau$$

where:

$$g(t) = \frac{a_0}{2} + a_1 \cos\omega_c t + a_2 \cos 2\omega_c t$$

$$\tau = \frac{1}{\omega_c}\cos^{-1}\frac{\alpha_0 - \alpha_M}{\alpha_m A_c}, \qquad \tau \le \frac{T}{2}$$

We note in passing that, if $\tau = \frac{T}{2}$

$$a_0 = 2\alpha_0$$

$$a_1 = -\alpha_m A_c$$

$$a_2 = 0$$

then

$$g(t) = \alpha_0 - \alpha_m A_c \cos\omega_c t \qquad \text{(N1-4)}$$

which is equation (4) forming the basis of the calibration analysis.

In contrast, if $\tau = \frac{T}{4}$, we expect a worse case condition with maximum second harmonic of the calibration frequency. Then

$$\tau = \frac{T}{4}$$

$$a_0 = 2\alpha_0 - \frac{4}{\pi}\alpha_m A_c$$

$$a_1 = 0$$

$$a_2 = -\frac{4}{3\pi}\alpha_m A_c$$

and

$$g(t) = \alpha_0 - \frac{2}{\pi}\alpha_m A_c - \frac{4}{3\pi}\alpha_m A_c \cos 2\omega_c t \qquad \text{(N1-5)}$$

Therefore, for the case where we have symmetrical operation about the z(t) = 0 axis of the transfer gain response, the calibration signal at frequency ω_c will be zero. Operation of the ferrite modulator will take place somewhere between the design operation of equation (N1-4) and the worse case operation of equation (N1-5). We wish to calculate the amplitude of the first harmonic a_1 as a function of the bias level which, in turn, determines the relative location of τ. The amplitude dependence of a_1 will then indicate the error in the calibration signal in terms of the operating point α_0. It will be convenient to calculate the amplitude a_1 in terms of the 'normalized' bias point given in equation (N1-2). Then,

$$b \equiv -\cos\omega_c\tau = \frac{\alpha_M - \alpha_0}{\alpha_m A_c} \qquad \text{(N1-6)}$$

Clearly, the maximum value of b is unity and occurs when

$(\alpha_M - \alpha_o) \geq \alpha_m A_c$ or when operation is strictly in the first quadrant of the gain transfer response. When $b = 1$, $\tau = \frac{T}{2}$ and equation (N1-4) applies with the amplitude of the first harmonic $a_1 = \alpha_m A_c$. From equations (N1-3) and (N1-6), a general expression for a_1 in terms of b is the following.

$$a_1 = \alpha_m A_c \left[-\frac{2b}{\pi} (1 - b^2)^{1/2} + 1 - \frac{2}{\pi} \cos^{-1}(-b) \right] \qquad \text{(N1-7)}$$

and similarly for a_o

$$a_o = \frac{4}{\pi} \alpha_m A_c \left[-b \cos^{-1}(-b) - (1 - b^2)^{1/2} \right] + 2\alpha_M + 2b\,\alpha_m A_c$$

The table below shows the values of a_o and a_1 as a function of b.

b	a_o	a_1
1	$2\alpha_M - 2\alpha_m A_c = 2\alpha_o$	$-\alpha_m A_c$
0.866	$2\alpha_M - 1.798\,\alpha_m A_c$	$-0.9425\,\alpha_m A_c$
0.5	$2\alpha_M - 1.44\,\alpha_m A_c$	$-0.61\,\alpha_m A_c$
0.2	$2\alpha_M - 1.3\,\alpha_m A_c$	$-0.245\,\alpha_m A_c$
0	$2\alpha_M - 1.275\,\alpha_m A_c$	0

We may now plot the amplitude of the calibration signal a_1 as a function of the 'normalized' ferrite modulator bias point α_o. This is shown in the figure below.

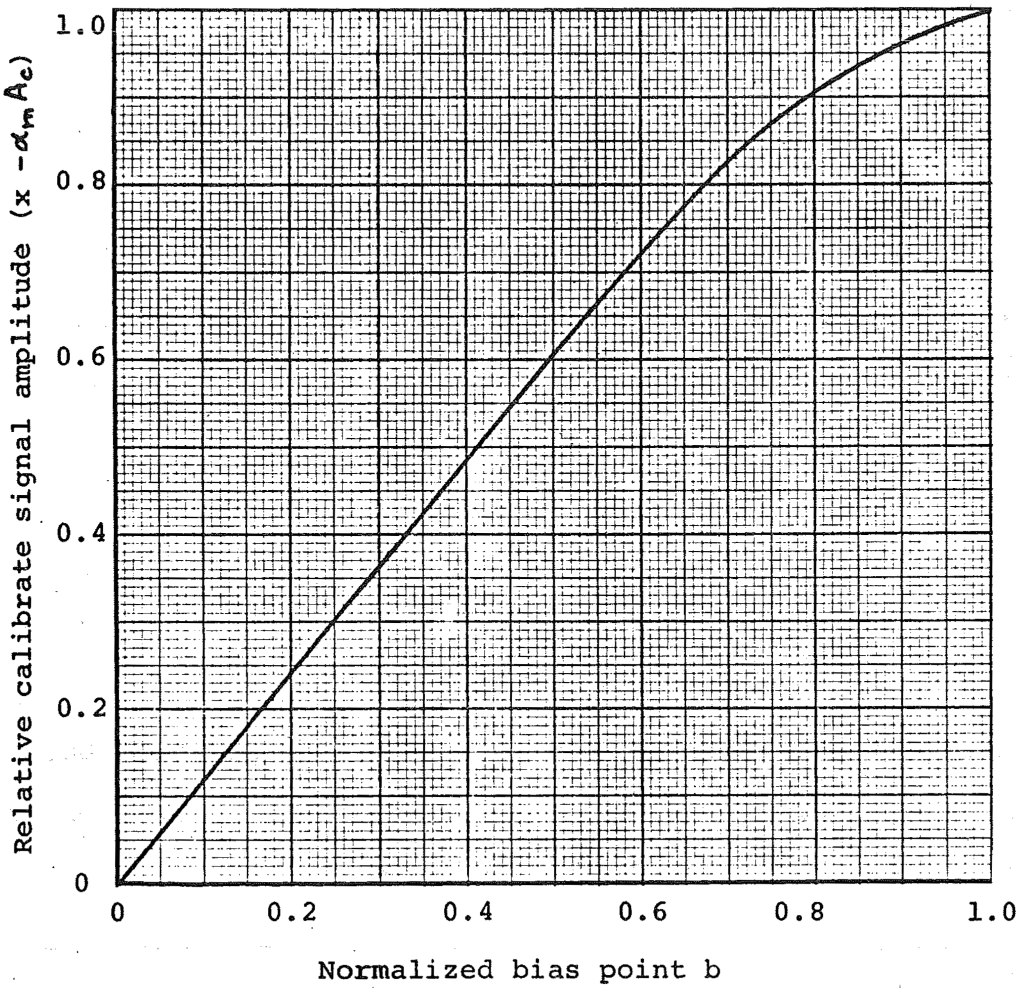

Relative Amplitude of the Calibration Signal as a function of the normalized bias point b.

$$b = \frac{\alpha_M - \alpha_o}{\alpha_m A_c} \quad , \; b \leq 1$$

α_M = maximum gain of the ferrite modulator

α_o = operating bias point

α_m = gain transfer response

We now wish to relate the error in the calibration signal to the error in the scattering coefficient σ^0. The relation between the recorded calibration signal E_r and σ^0 is given in the expression below.

$$\sigma^0 = \text{(other terms)} + 20 \log_{10} \frac{E_s}{E_r}$$

where: E_s = measured signal voltage

E_r = calibration voltage

If we have an error δ in the calibration voltage, then the error in the calculation for σ^0 will be

$$\begin{aligned}\Delta\sigma^\circ &= -20 \log_{10} (E_r + \delta) + 20 \log_{10} E_r \\ &= -20 \log_{10} \frac{E_r + \delta}{E_r} = -20 \log_{10} \frac{k \alpha_m A_c}{\alpha_m A_c} \\ &= -20 \log_{10} k \qquad \text{(N1-8)}\end{aligned}$$

where k is the coefficient of the a_1 term derived above. The table below shows the variation of $\Delta\sigma^0$ calculated as a function of the normalized bias point b.

b	a_1	k	$\Delta\sigma^0$
1	$-\alpha_m A_c$	1	0
0.866	$-0.9425\alpha_m A_c$	0.9425	0.5 dB
0.5	$-0.61\ \alpha_m A_c$	0.61	4.28
0.2	$-0.245\ \alpha_m A_c$	0.245	12.2
0	0	0	∞

The error in scattering coefficient $\Delta\sigma^0$ is plotted as a function of the normalized bias point b in the figure below.

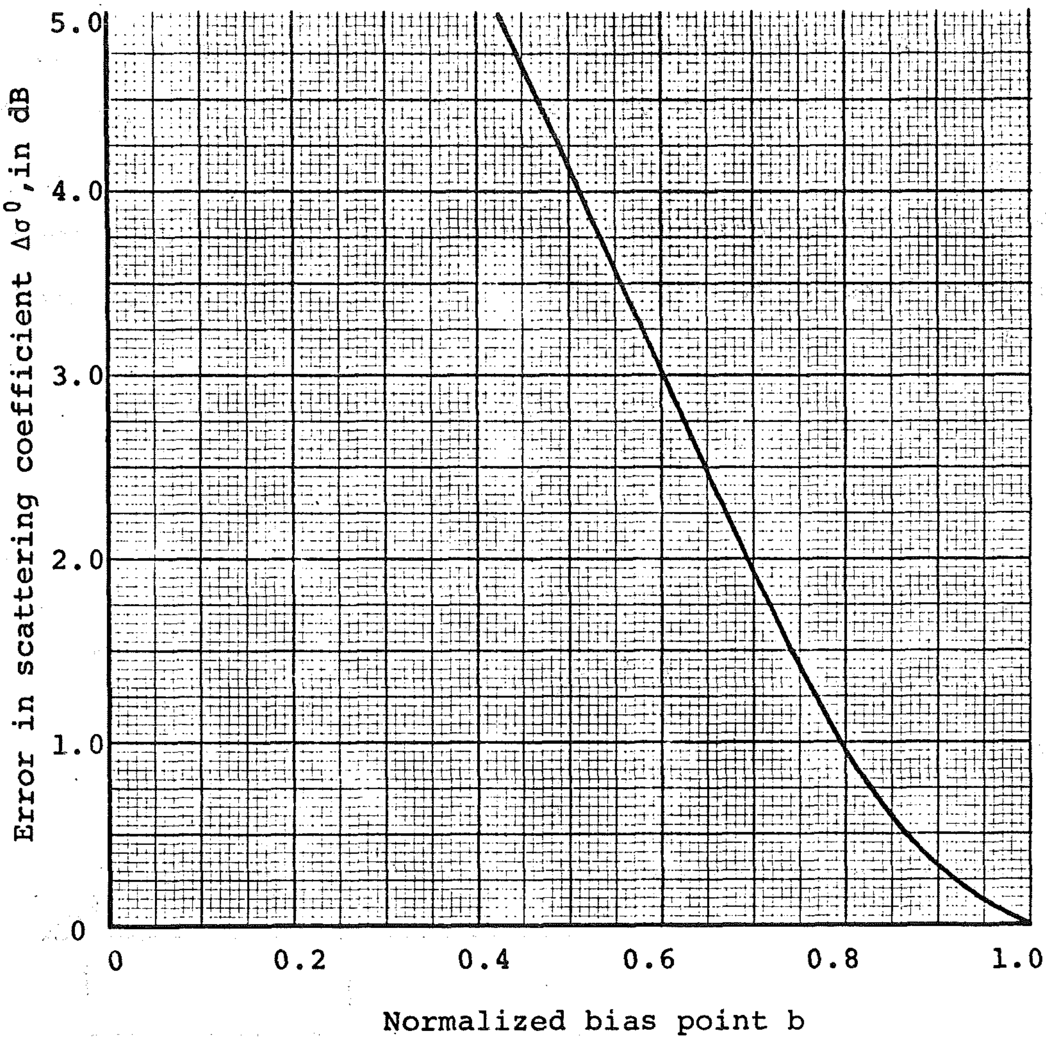

Scattering coefficient error as a function of the normalized bias point of the ferrite modulator.

Because of the dramatic increase in scattering coefficient error as b decreases it is concluded from this analysis that operation of the ferrite modulator must be constrained by a fixed bias to a linear region of the first quadrant of the gain transfer response.

B. PIN diode modulator using square-wave modulating signal.

The transfer 'gain' of the PIN diode modulator is plotted as a function of input voltage v(t) in the figure below. The maximum gain α_M again occurs when v(t) = 0. Because the operation is designed to provide either maximum or minimum (assumed here to be zero) gain, the bias point is selected at $\frac{1}{2}\alpha_M$.

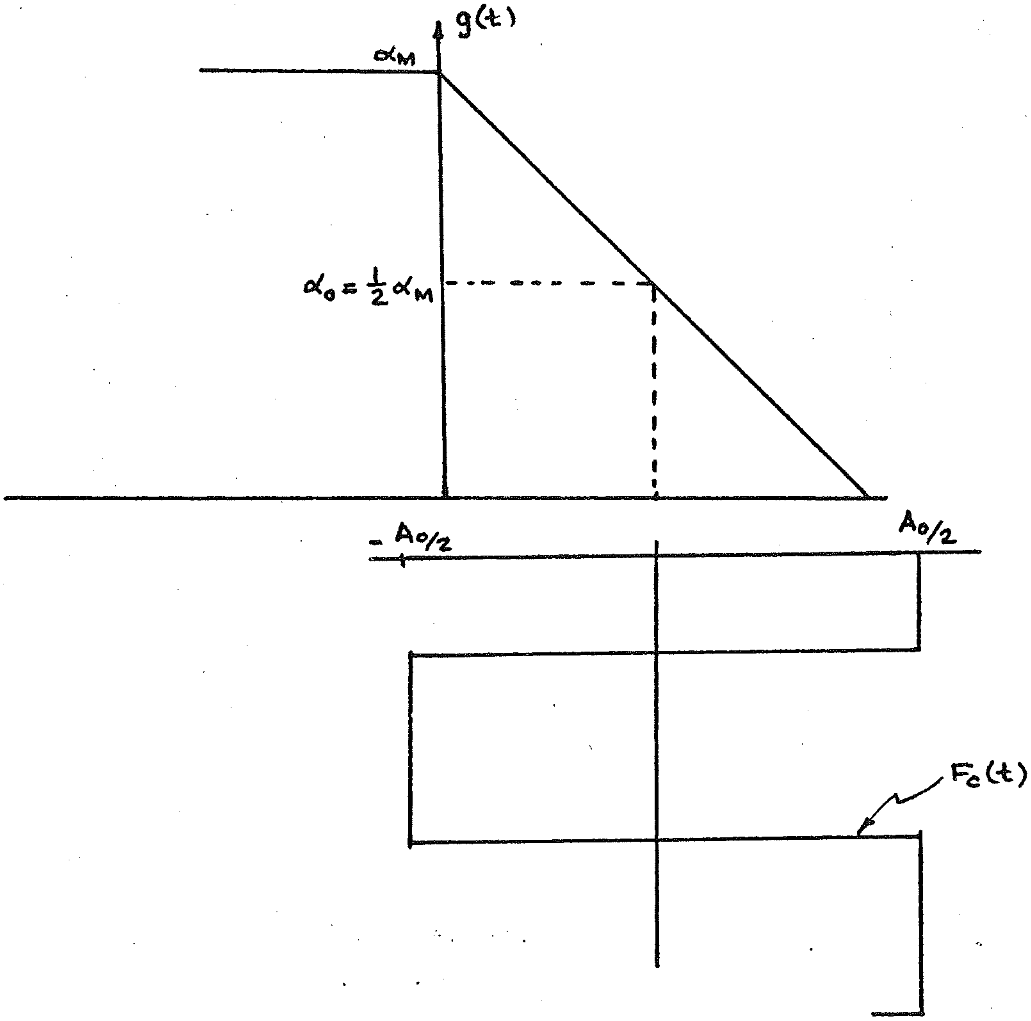

It was shown in Appendix II that the Fourier expansion of the square wave yields a first harmonic term of

$$F_c(t) = \frac{2A_o}{\pi} \cos \omega_c t$$

We note from the figure above that, as long as the amplitude $A_o/2$ of the square wave is of sufficient magnitude, the dynamic gain term $\alpha_m F_c(t)$ of equation (II-1) will assume the form

$$\alpha_m F_c(t) = \frac{2\alpha_M}{\pi} \cos \omega_c t$$

and with a bias located at $\frac{1}{2}\alpha_M$ the total modulating 'gain' will be

$$\left(\alpha_o - \alpha_m F_c(t)\right) = \alpha_M \left(\frac{1}{2} - \frac{2}{\pi} \cos \omega_c t\right)$$

as used in equation (II-6) of the analysis in Appendix II. This waveform is sketched in the figure below.

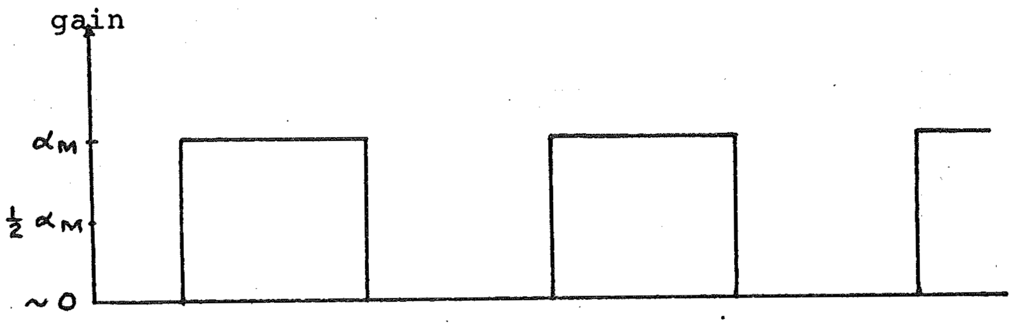

NOTE II. On the use of a non-ideal square wave.

Suppose that a non-ideal square wave is used as the modulating signal for the PIN diode injection design. It is easy to see that the greatest error in the calibration system occurs when the leading and trailing edges of the 'square wave' have a sinusoidal shape at the fundamental, or calibrate, frequency. For our analysis of the relationship between calibration signal error and the shape of the modulating waveform, we will use a cosine wave limited in amplitude as shown in the figure below.

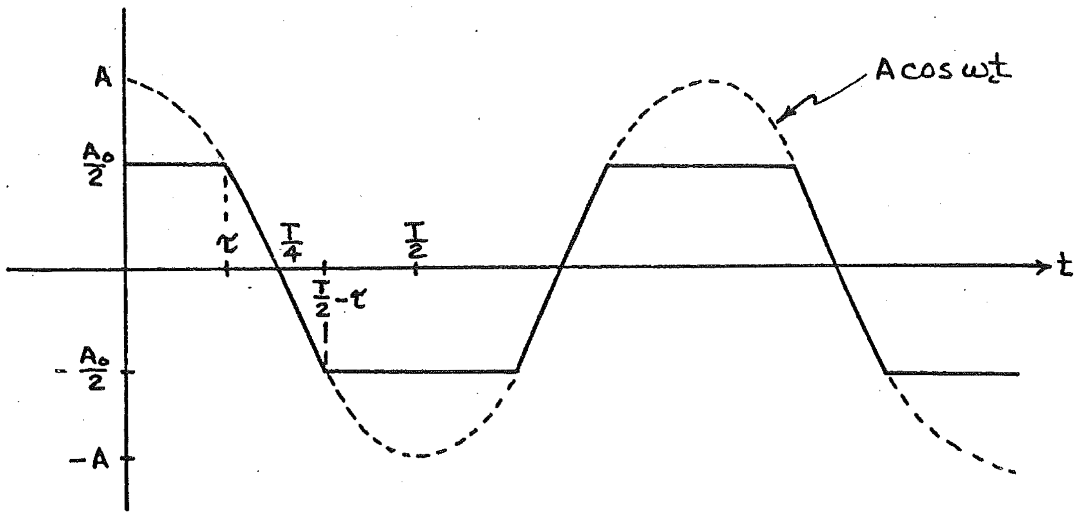

Expanding the distorted square wave as a Fourier series, it is a straightforward exercise to calculate the coefficients. Then, in summary

$$f(t) = \frac{a_o}{2} + \sum_{n=1}^{\infty} a_n \cos n\omega_c t$$

where:

$$a_0 = 0$$

$$a_1 = \frac{2A_0}{\pi} \sin \frac{2\pi}{T}\tau + A\left[1 - \frac{4}{T}\tau - \frac{1}{\pi}\sin\frac{4\pi}{T}\tau\right]$$

and, for n even, $a_n = 0$

for n odd,

$$a_n = \frac{2A_0}{n\pi} \sin n\frac{2\pi}{T}\tau - \frac{2A}{\pi}\left[\frac{\sin(n+1)\frac{2\pi}{T}\tau}{(n+1)} + \frac{\sin(n-1)\frac{2\pi}{T}\tau}{(n-1)}\right]$$

Again, the only frequency term of interest is that at ω_c.

$$f(t) = \frac{2A_0}{\pi} \sin \frac{2\pi}{T}\tau \cos \omega_c t$$

$$+ A\left(1 - \frac{4}{T}\tau\right)\cos \omega_c t - \frac{A}{\pi}\sin\frac{4\pi}{T}\tau \cos \omega_c t$$

In order to compute the error in the calibration signal, we must compare f(t) with $F_c(t)$ derived in Note I above.

$$F_c(t) = \frac{2A_0}{\pi} \cos \omega_c t$$

$F_c(t)$ represents the ideal square wave. For this analysis, we will assume an amplitude A of the sinusoid, then compute the error in calibration signal as a function of A. We will then relate this amplitude to the rise time of the distorted square wave.

Let $\quad A = 20\ A_o/2 = 10\ A_o$

Then, to calculate τ

$$A \cos \frac{2\pi}{T} \tau = \frac{A_o}{2}$$

$$\cos \frac{2\pi}{T} \tau = \frac{1}{20} = 0.05$$

$$\frac{\tau}{T} = 0.242$$

and

$$f(t) = \frac{2A_o}{\pi} \cos \omega_c t + 0.0025\, A_o \cos \omega_c t$$

The error in the calibrate signal amplitude is then

$$\frac{0.0025\, A_o}{\frac{2A_o}{\pi}} \times 100 = 0.4\ \%$$

The rise time corresponding to this maximum error is obtained by reference to the figure sketched below.

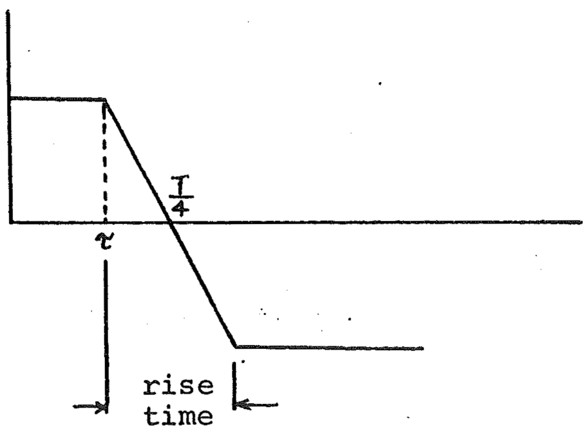

$$\text{rise time} \equiv t_r = 2\left(\frac{T}{4} - \tau\right)$$

$$= 2(.25T - .242T)$$

$$= 0.016T \quad .$$

As an example, let the calibrate signal frequency be 10 kHz. Then, $T = 10^{-4}$ seconds and the rise time t_r = 1.6 microseconds for a maximum calibrate signal error of 0.4 %. The above analysis can be used to predict the error in the calibrate signal for a given square-wave rise time.